Quaternary groundwater history in south-eastern Australia: Lake Sunrise, NSW.

Jack Flanagan

Department of Earth and Environmental Sciences

Faculty of Science of Engineering

Macquarie University, Sydney, NSW 2109

October 6, 2021

A thesis submitted in partial fulfillment of the requirements for the degree of Master of Research

Declaration

I hereby declare that this Master of Research thesis has not been submitted to any other institution or university for a higher degree. This thesis is comprised entirely of my own work, except where otherwise acknowledged. There were no ethics considerations which required approval for this thesis. This thesis is formatted as a manuscript for submission to the *Journal of Quaternary Science,* with some exceptions to meet the requirements of the Macquarie University. This includes the requirement of an abstract of 200 words, 2cm margins, 1.5x line spacing, figures and tables embedded within the text.

Jack Flanagan

6th October 2021

Contents

Acknowledgments……………………………………………………………………………………………...v

Covid impact statement………………………………………………………………………………………..vi

Abstract...vii

1 Introduction

1.1 Quaternary Lake systems…………………………………………………………………………………….1

1.2 Aims and hypothesis……………………………………………………………………………………….4

1.3 Site introduction…………………………………………………………………………………………….5

1.3.1 The Lake Sunrise Basin………………………………………………………………………………...5

1.3.2 Modern climate……………………………………………………………………………………….....6

1.3.3 Vegetation…………………………………………………………………………………………….....6

1.3.4 Geology in the Lake Sunrise region…………………………………………………………………….6

1.3.5 Current groundwater setting and recent trends…………………………………………………………...6

1.4 Methods……………………………………………………………………………………………………..9

1.4.1 Field site and methods………………………………………………………………………………….9

1.4.2 Sedimentology methods…………………………………………………………………………………...9

1.4.3 Dating methods………………………………………………………………………………………...10

2 Results - sedimentology

2.1 Sedimentology results……………………………………………………………………………………...11

2.1.1 textural analysis…………………………………………………………………………………………..11

2.2 Modal grain size analysis / sediment facies description………………………………………………………..12

2.3 Core analysis………………………………………………………………………………………………...14

2.4 Site depositional analysis……………………………………………………………………………………18

3 Results – age estimation

3.1 Single-grain quartz D_e distributions……………………………………………………………………………..20

3.2 Grain screening and rejection criteria…………..……………………………………………………………….22

3.3 Environmental dose rate…………………………………………………………………………………………22

3.4 Final OSL age estimation……………………………………………………………………………………...23

4 Discussion – Age estimation

4.1 Model selection……………………………………………………………………………………………….25

4.2 OSL age vs depth modelling…………………………………………………………………………………...27

4.3 Water content estimation……………………………………………………………………………………………28

5 Discussion – Palaeoenvironmental reconstruction of the Lake Sunrise Basin

5.1 Classification of sediment facies………………………………………………………………………………...30

5.2 Lake formation and chronostratigraphy…………………………………………………………………………...33

5.2.1 Chronology of lake formation – phase analysis……………………………………………………………………..35

5.3 Hydrological balance of Lake Sunrise……………………………………………………………………………..43

5.4 Groundwater response to Quaternary hydrological change in south-eastern Australia………………………46

5.4.1 MIS5……..46

5.4.2 MIS4……..46

5.4.3 MIS3……..47

5.4.4 MIS2……..47

5.4.5 MIS1……..48

6 Conclusions and recommendations

6.1 Conclusions…………………………………………………………………………………………………...50

6.2 Recommendations……………………………………………………………………………………………...50

7 References……………………………………………………………………………………………………51

8 Appendix

8.1 Water balance calculation results table……………………………………………………………………….59

8.2 Radial plots……………………………………………………………………………………………………….62

Acknowledgements

There are many people to thank! I would firstly like to thank my two supervisors. Associate Professor Paul Hesse has been instrumental in developing my understanding, technical training and passion for sedimentology and Quaternary sciences. I am extremely appreciative of his ongoing support and guidance throughout my research project. Associate Professor Kira Westaway has also been very supportive, particularly with the technical training and data analysis associated with OSL, as well as general mental support, for which I am extremely thankful. Secondly, I would like to thank my dear friend Levente Laczko. He has provided a massive amount of field assistance, lab guidance and motivation throughout our 6 years studying together, cheers mate. I would like to also thank Molly Quinn and Sam Shumack for their assistance with all things OSL and GIS. My best mates Zach, Andre and particularly Josh have all supported me throughout my Masters program, thanks lads. A very special thank you to my grandparents Patrick and Glenys Flanagan. Allowing me to conduct fieldwork for my thesis on the family property 'Sunrise' has been truly special, it is always a place that I will hold close to my heart.

And finally, to my parents and sister. Thank you all for your ongoing support throughout my studies, particularly during COVID. I'm blessed to have the undying support of you all, and I will be eternally grateful.

Patrick, Paul and Jack at Lake Sunrise, 2020.

Candidate's statement about the impact of COVID-19 changes on the thesis

Dear Examiner,

Many of our HDR candidates have had to make changes to their research due to the impact of COVID-19. Below you will find a statement from the candidate, approved by their Supervisory Panel, that indicates how their original research plan has been affected by COVID-19 restrictions. Relevant ongoing restrictions in place caused by COVID-19 will also be detailed by the candidate.

Candidate's Statement

The COVID crisis has presented numerous challenges whilst completing my thesis. The closure of the University labs, supply chain delays, cancellation of fieldwork and the challenges of working solely from home, as a result of COVID, have all impacted my thesis. The rush to finish lab work and process data to try avoid the lockdown period is reflected in some of the results in this thesis. The OSL results took a particular hit, as the sample preparation and analysis time had to be rushed, resulting in less grains (as well as total samples) analysed. The COVID travel restrictions also meant that only a single field work trip could occur, resulting in suboptimal sampling locations and depths in some of the cores. Some speculation within the discussion is largely attributed to the sampling, limited by the single field trip.

Abstract

The Murray-Darling Basin of south-eastern Australia contains a trove of rich paleoenvironmental relicts, representing the unique hydroclimatic conditions under which they formed. Lake systems contain sediment archives of depositional history in their nearshore and bordering dune (lunette) geomorphic landforms. Fluctuating periods of high lake levels with intermittent periods of deflation (and subsequent dune building) can be interpreted from the high-resolution stratigraphy preserved within these landforms. An ephemeral groundwater discharge lake, known as Lake Sunrise, lacking major fluvial connectivity, was chosen for this study. Nearby lake basins, such as the Willandra Lakes complex, rely on fluvial inflows, as well as groundwater fluctuations to produce 'lake full' conditions, however this relationship is poorly understood. By contrast, due to its isolation, Lake Sunrise responds to fluctuations in the regional groundwater table. A stratigraphic framework based on particle size, mineralogy, and single-grain optically stimulated luminescence (OSL) age estimates was developed. A series of clay lunettes was analysed, revealing oscillating periods of enhanced groundwater discharge throughout the late Quaternary, from ~ 90 ± 4 ka - 24 ± 1 ka. Comparing these findings to other regional proxies reveal that groundwater discharge basins experience a ~10,000 – 20,000 year 'lag' between regional groundwater recharge and surface discharge.

1. Introduction

1.1 Quaternary Lake systems

The Australian landscape is a haven for Quaternary environmental reconstructions. The low relief coupled with prolonged tectonic stability has assisted in preserving high-resolution evidence of past environmental changes (Bowler, 1978) in response to the orbital variations of Milankovitch cycles (Emiliani, 1966). The environmental evolution of the Murray-Darling basin in south-eastern Australia is of particular interest, as the responses of hydrological systems to climatic forcing throughout the Quaternary, particularly surface water availability, help us to understand the evolution of modern water resources in response to anthropogenic climate change and land use.

The Murray-Darling Basin in South-eastern Australia contains a rich archive of relict geomorphic land features which have been used as proxies for late Quaternary environmental change, including palaeochannels (Page et al., 1996; Hesse et al., 2018), lacustrine lunette systems (Bowler et al., 2003; Fitzsimmons et al., 2014; Jankowski et al., 2020) and source-bordering dunes (Kemp and Rhodes, 2010), all of which can be used to infer changes to surface palaeohydrology and aeolian activity. Evidence from Murrumbidgee palaeochannels active during MIS 5, 3 and 2 reveal enhanced hydrological activity on the Murray-Darling Basin, with the bankful discharges in the order 3 – 270 times the magnitude of their modern equivalents (Hesse et al., 2018). Further to the west, Lake Mungo is perhaps the most studied and significant lacustrine archive in Australia. Sedimentological records from the source bordering dunes (lunettes) of Lake Mungo contain a high-resolution chronostratigraphic archive of sandy beach ridges and deflated clay lakebed material, formed through the coupled cycle of rising water levels and desiccation in response to variable catchment discharge (Barrows et al., 2020; Jankowski et al., 2020). This site is also significant due to its evidence of anatomically modern human inhabitation on the Australian continent, with the archaeological remains of the 'Mungo Man' found at a cremation site in the southern lunette, predating 40 ka (Bowler et al., 1970; Bowler et al., 2003).

Water levels at Lake Mungo are predominantly reflective of the surface discharge from its supplying fluvial system, i.e. Willandra Creek, a palaeochannel of the modern-day Lachlan River (Kemp et al., 2017; Jankowski et al., 2020). Thus, Lake Mungo is mainly a proxy of the hydrological variability of the Willandra Creek up until 14 ka, (and Lachlan River) catchment, rather than water availability in the local area (Bowler et al., 2012). Bowler (et al., 2012) asserts that groundwater discharge plays a significant role in the hydrological activation of Lake Mungo. As surface waters recede, following periods of increased fluvial discharge, seasonal groundwater discharge dominates lake hydrology and its salinity aids the deflation of clay-rich sediment from the lakebed (Bowler et al., 1998; Bowler et al., 2012). Understanding the history of groundwater discharge in these lake basins is complex, particularly when separating it from other inputs, namely surface runoff and direct precipitation. Whilst the volume of water in a connected ephemeral lake system primarily reflects the fluvial system supplying it, the role and temporal variability of groundwater in such lake systems is difficult to isolate. In contrast, hydrologically isolated lake systems, are dominated by groundwater inputs and outputs because runoff is minimal. Bowler (1998) explains that groundwater shares an intrinsic 'lagged' relationship with available surface water, rate than the availability of surface water filling a lake system. The mechanisms behind such processes are poorly understood, and the temporal scales at which this lag operates is relatively unknown.

In order to truly understand the response of groundwater systems to Quaternary environmental change, a site with minimal or no surface water inflow was required. Lake Sunrise on the Riverine Plain was selected for this study. It resides in a small catchment with no visible or modelled connectivity to the Lachlan or Murrumbidgee rivers and contains three visible lunettes. A stratigraphic and sedimentological analysis, paired with OSL age estimation was used to reconstruct the hydrological history of the lake basin as a proxy for groundwater level and discharge. A nearby unstudied palaeochannel of the Murrumbidgee River, named here as the Sunrise palaeochannel, is also dated in this thesis. It is hydrologically disconnected from the Lake basin and hence serves as an indicator of regional surface hydrological activity.

Lake source bordering dunes – the 'lunette'

The geochemistry and sedimentology of lunette sediments is the primary avenue for ascertaining the prevalence of groundwater discharge in Quaternary Lake basins in Australia, such as Prungle Lakes (Magee, 1991) and Lake Mungo (Bowler et al., 2012). The efflorescence of salts and subsequent aggregation of clay sized particles leads to the formation of clay 'pellets', a function of hypersaline groundwaters evaporating during relatively dry hydroclimatic phases (Bowler and Teller, 1986). These pellets are typically sand sized, capable of saltation during periods of lakebed deflation, and deposited in the downwind dune structures. In Australia, these pellets are well preserved in dunes of many ancient lake complexes, namely throughout the south-eastern part of the continent (Bowler, 1973). The preservation of these pellets in ancient dune structures (Bowler, 1986, Jankowski et al., 2020) and absence in most modern Australian lake systems is further evidence of their presence in a narrow window of evaporite-conducive conditions. However, a small number of examples of modern pelletal clay formation occur in Australia. Lake Tyrrell, in north-western Victoria, is a hypersaline ephemeral basin with a high annual rate of seasonal desiccation, surface brine exposure and evaporite formation. These features of the lake provide optimal conditions for the precipitation of gypsum and other salts to form clay pellets (Bowler and Teller, 1986). Similar modern processes occur in other arid/ semi-arid regions including Texas (Huffman and Price, 1949), Namibia (Brook et al., 2007) and Tunisia (Coque, 1962), providing an environmental window into the drastically different conditions experienced in south-eastern Australia in the late Quaternary.

The classification of source-bordering dunes in the literature extends back to the mid-20th century. Termed *"source-bordering lee dunes"* (Melton, 1940), interpretations of the nature and origin of these dunes were limited to visual examination and were limited in detail. Melton determined the basic formation mechanism of source-bordering dunes to be the deposition of fluvial / lacustrine sediments on the leeward (downwind) side of an area dominated by loose sand, with a particular emphasis on the persistence of wind that possesses an 'unvarying' direction. Such accumulation is probably a result of a persistent, unimodal wind regime (Sankey et al., 2018) but, is dependent on the availability of sediment to be reworked. Wind strength does not appear to play a major role in the formation of these dunes, as is the case with the majority of sand dune types (Wasson and Hyde, 1983), rather, wind direction plays a more substantial role in the formation process. Lacustrine source bordering dunes will often form transverse to the persistent wind regime, leading to a dune sitting parallel to the shoreline. Research into the formation of clay-dominated source bordering dunes (Price, 1963) shed light on dune formation mechanisms, with Price hypothesising about periods of *'deflation'* (aeolian erosion of loose material) driving periods of dune formation in clay-enriched basins.

Clay dunes differ greatly from their quartz dune cousins. They occur proximal to their source, typically on the fringing margins of groundwater discharge basins, often conforming to the shape of the sourced area. In the instance of a round ephemeral lake system, a crescentic lunette can be found on the downwind shoreline. They typically range from 5-15 m in height, although examples of clay dune crests rising over 30 m are known (Bowler, 1971). While similar in gross morphology, Bowler noted that crescentic sand (barchan) dunes are highly mobile, with leeward facing horns. In contrast, the typical clay dune is immobile, and the trailing sides face windward. This is typical of most lunettes in south-eastern Australia, which are both rich in sands and clays, as presented by Bowler (1971) whereby a sandy lunette is encroached by a younger clay dune, forming a compound lunette. This presented model is interesting, as the morphologies of compound dunes next to lake basins are almost always lunette-like it nature, regardless of the presence of sand or clay in varying proportions. Such an example can be seen at Lake Urana in NSW where the primary dune composition is coarse sand (Page et al., 1994). This is because the underlying sand dune is a foredune, also intrinsically linked to the shoreline when water levels are high. Thus interpreting the sedimentology of these dunes reveals the lake level status in the past. The post depositional behaviour of pelletal clays in situ is subject to much speculation. Micro-sedimentological analysis of cores from Lake Mungo, NSW reveal the complex issues associated with interpreting environmental history based on stratigraphy, particularly as processes of chemical weathering break down the pelletal form of the clay, removing evidence of the groundwater controlled environment under which they were deposited (Jankowski et al., 2020). Pedogenesis is also responsible for the illuviation of clay minerals. Increase in water availability on the dune surface following rain enhances the percolation of clays. These processes, when coupled with bioturbation, provide optimal conditions for pelletal clay destruction (Fitzsimmons et al., 2007), as well as secondary recrystallisation of gypseous minerals (Magee, 1991). Bowler (et al., 2012) also highlights the 'flushing effect' of freshwater inflows, removing gypseous evaporites that are stored on the lower shore front of lunettes, and are a primary source of evidence used to infer the presence of groundwater in a lake system and form clay pellets. Thus, caution must be taken when interpreting pelletal clay facies in relic landforms. By removing the uncertainty of relying on geochemical analysis (and reliance on pelletal clays) the primary objective of this thesis is to understand the prevalence of groundwater in a lake system, A more robust understanding of the temporal scales over which groundwater discharge systems operate can thereby be achieved.

1.2 Aims and hypothesis

This thesis addresses the research question: ***"How has the temporal availability of groundwater in closed lake systems responded to Quaternary environmental change in South-Western NSW?"*** testing the hypothesis that groundwater level is higher following periods of enhanced/extended surface hydrological activity. This hypothesis will be tested at Sunrise Lake, a small, isolated lake between the Murrumbidgee and Lachlan fans in the Murray Basin. This lake serves as an independent limnological archive of groundwater fluctuations, in a region that appears protected from the geomorphic influence of distributive fluvial systems (DFS).

Specifically, the aims of this thesis are:

Groundwater surface exposure – Understanding the site evolution of the Lake Sunrise basin using a chrono-stratigraphic and sedimentological approach.

Lake volume and geometry – Modelling the geometry of the lake to understand what kind of hydrological regime it takes to fill the lake; at what point does it overflow? What is the supplying catchment? How does it compare with lakes within the same region?

Lake level fluctuation – Using sedimentological and age analysis to understand the rate at which lake levels fluctuate at this site, differentiating the role of surface and groundwater in such fluctuations using a multi-proxy approach.

Significance of study

To the present, the relationship between surface and sub-surface hydrology has often been overlooked. There are two major constituents to this study that make it highly relevant for Australia's Quaternary environmental reconstruction:

Providing an independent environmental record– This lake system drains a small, isolated catchment, void of influence from nearby major fluvial systems; the Lachlan and Murrumbidgee Rivers. Hence, groundwater must be the primary source of discharge to the lake. Through analysis of the evolution of Lake Sunrise, the response of groundwater fluctuations to Quaternary environmental change can be identified. This will shed light on the role of groundwater in intensively studied lacustrine systems such as the Willandra Lakes in future studies.

Enhancing the Riverine Plains chronology – The addition of ten unpublished optically stimulated luminescence (OSL) ages will assist in further developing our understanding of the Quaternary evolution of the Murray-Darling basin.

1.3 Site introduction

1.3.1 The Lake Sunrise Basin

Lake Sunrise is an ephemeral closed lake system in the semi-arid zone of south-eastern New South Wales, Australia. The lake sits in a unique low-lying pocket between the alluvial fans of the Murrumbidgee and Lachlan distributive fluvial systems, which has been prone to groundwater discharge at various stages through the late Quaternary. The lake bed sits 91 mASL whilst the highest peak of the largest lunette reaches 103 mASL with flow-route modelling suggesting that the closest (unstudied) palaeochannel of the Lachlan River ~ 6 km NW and newly dated (this thesis) palaeochannel of the Murrumbidgee River ~ 4 km to the SE are unable to flow into the Lake Sunrise basin under the current climatic and hydrogeological setting (Fig 1.3.1).

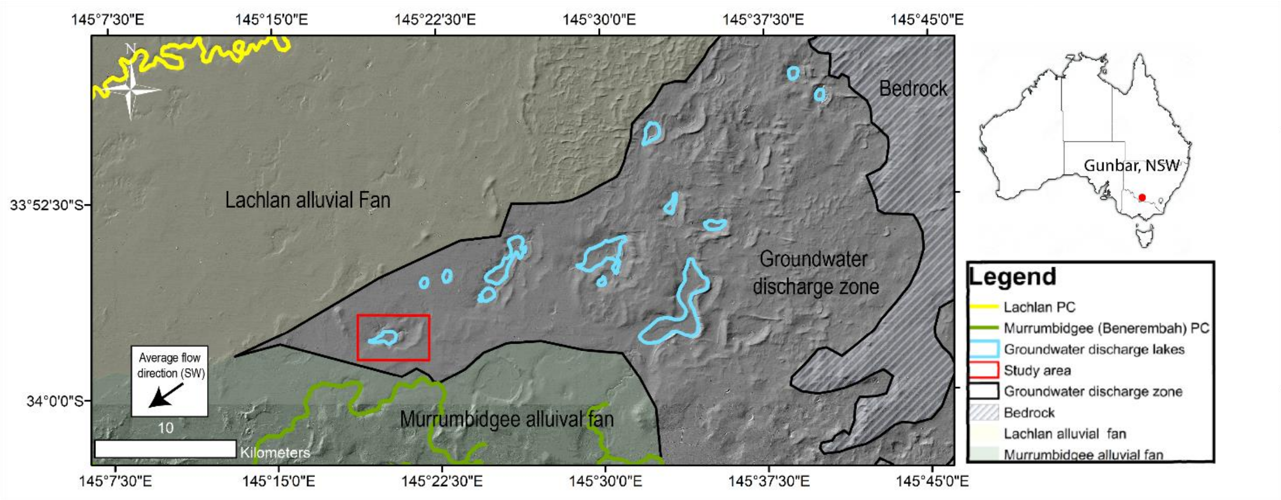

Figure 1.3.1 – Location of Lake Sunrise in New South Wales, Australia. The lake sits in a groundwater discharge zone (purple outline) wedged between the extent of the Lachlan River alluvial fan and Murrumbidgee River alluvial fan. The light blue areas represent the lakes in the groundwater discharge zone. Palaeochannels sourced from Hesse (et al., 2018). The average flow direction is oriented towards the south-west. Data for major MDB rivers (right) sourced: NSW Hydrography, 2021.

There have been various configurations of Lake Sunrise throughout the Quaternary (Figure 1.3.4). In its smallest configuration (inner lunette complex) the Lake surface area is ~ 1.15 km^2, whilst the largest configuration of the lake (outer lunette complex) is ~ 7.01 km^2 both supplied by a catchment area of 69.2 km^2. The irregular catchment, determined using flow direction, flow accumulation and watershed hydrological modelling tools in ArcGIS and the NSW 5m DEM, is the result of the very flat terrain with numerous small lakes acting as local sinks for runoff. No stream channels occur in the catchment area outside the lake areas, however, small local gullies do convey runoff into the lake basin during rainfall events. A nearby palaeochannel of the Murrumbidgee River (figure 1.3.1) ~ 4 km from the lake basin (but disconnected) is also investigated in this thesis, used as an indicator of surface hydrological. Initial mapping suggests that this palaeochannel may be an extension Benerembah arm that diverges from the modern Murrumbidgee River at Darlington Point, NSW.

1.3.2 Modern climate

This region of the Murray-Darling Basin is semi-arid, with average annual rainfall in the basin (over a 30 year period) 372 mm and evaporation rates ~ 2000 mm/year (Australian Bureau of Meteorology, 2021). This area is characterised by very hot summers (YTD maximum – 41.7 °C, 30-year average 24.4 °C) and cool winters (YTD minimum: - 1.8 °C, 30-year average: 9.5 °C) (Australian Bureau of Meteorology, 2021). Wind speed and direction data from the Hay weather station 77 km away

(Australia Bureau of Meteorology, 2021) shows predominantly south to south-westerlies year-round (since 1957) at an average speed of 10 – 20 km/h. Observations from landholders suggest that the lake basin has not filled since the first grazing operation commenced (1882), with all surface runoff recharging into the local aquifer or being quickly evaporated. The nearby palaeochannel pools water during large precipitation events however, the water does not flow.

1.3.3 Vegetation

The land surrounding the lake has been extensively modified for cropping and grazing. In the areas that have not been modified, vegetation is sparse, with some low exotic shrubs such as 'Crows foot' (*Eleusine indica*), 'Riverina blue bell' (*Echium plantagineum*) and 'Saltbush' (*Atriplex nummularia*) which sit amongst a small number of quite large Wilga trees (*Geijera parviflora*). Vegetation on the lake floor is far more concentrated, with a dense community of 'Black box gums' (*Eucalyptus largiflorens*), which are typically suited to dry, semi-arid woodlands, particularly in the saline soils of the Murray-Darling Basin (Slavich et al., 1999).

1.3.4 Geology in the Lake Sunrise region

The Lake Sunrise Basin sits on top of a number of well-documented geological units. The deepest unit is comprised of Devonian age undifferrentiated granite which is overlain by the Cainozoic basal group (Renmark Group Olney Formation), comprised of fluvio-lacustrine sourced, poorly sorted sediments, ranging from fine to gravelly sand (ga.gov.au, 2021). The medium-coarse sands of the Calivil formation, late Pliocene in age, follow and have been documented in drilling logs 10 km to the north of Lake Sunrise (WaterNSW, 2021). The Shepparton formation represents the final geomorphic evolution of the region before the inception of Lake Sunrise. Formed during subsidence in the Cainozoic period, the alluvial sediments or 'prior streams' from this formation are medium-coarse in nature and cover the majority of the Murray-Darling Basin (Brown and Stephenson, 1991). The isolation of Lake Sunrise sometime during the late Quaternary allowed for the reworking of the very upper sediments of the Shepparton unit, followed then by the formation of the modern day unconsolidated, red-brown clayey siliceous sand, rich in iron and carbonate cemented nodules, referred to as the Woorinen Formation (Geoscience Australia, 2021). Hydrological inactivity in the basin has allowed for the prolonged deposition deflated clays and silts on the lunettes, sourced from the exposed lake bed sometime during the late holocene.

1.3.5 Groundwater, current groundwater and recent trends

The Lower Lachlan Alluvium aquifer is a series of unconsolidated fluvial sediments deposited in the region surrounding Lake Sunrise. Two aquifer systems: a shallow (between 55 and 90 metres depth) and a deep (up to 400 m) system (figure 1.3.2) operate in the modern day and are notably disconnected from one another. The shallow aquifer is semi-confined to the Calivil formation, whilst the deepest aquifer is confined within the Renmark group sediments.

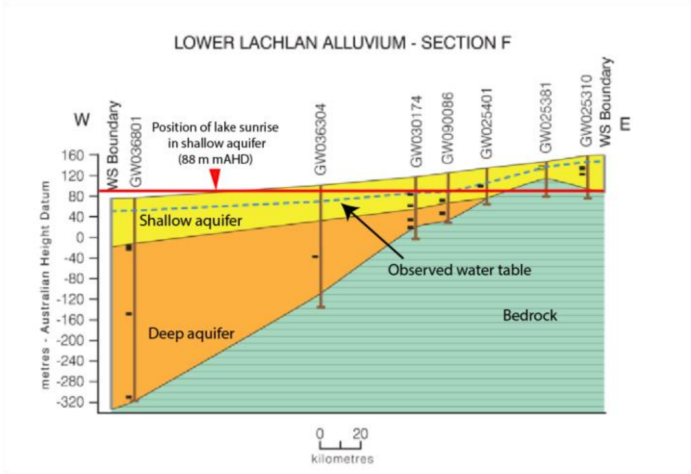

Figure 1.3.2 – Aquifer zones of the Lower Lachlan Alluvium, NSW (Department of Primary Industries, 2018). Readings are taken over a 200 km transect from Hillston (east) to the flat alluvial plain of the Lachlan River to the southwest. The shallow aquifer is semi confined to the Calivil formation whilst the deep aquifer is confined to the Renmark group sediments.

The most recent regionwide investigation of the Lower Lachlan Alluvium found the 2015/2016 standing water level varied from 25 – 40 metres below the surface, within the sediments of the semi-confined Calivil formation (NSW Department of Primary Industries, 2018). The shallow aquifer is responding to the increasing extraction rates for irrigation purposes. Figure 1.3.3 shows the water level from a groundwater bore in Hillston, NSW, falling deeper below the surface, approximtely 15 m during the 1994 – 2017 period. It is apparent that artifical extraction of aquifer water is causing the Lower Lachlan Alluvium to respond far more rapidly than is possible under any natural scenario, such as past climate changes. Further analysis of groundwater dynamics is outside the scope of this thesis.

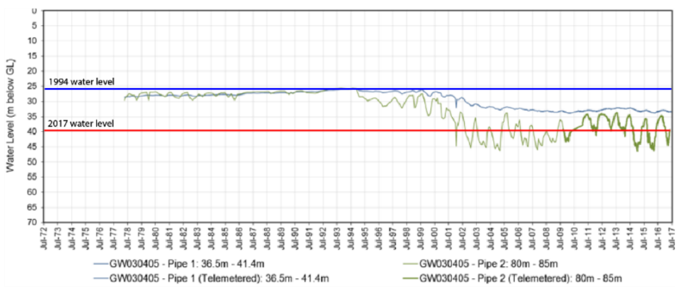

Figure 1.3.3 – Longterm Groundwater level variation since 1972. Hillston Groundwater monitoring station. (NSW Department of Primary Industries, 2018).

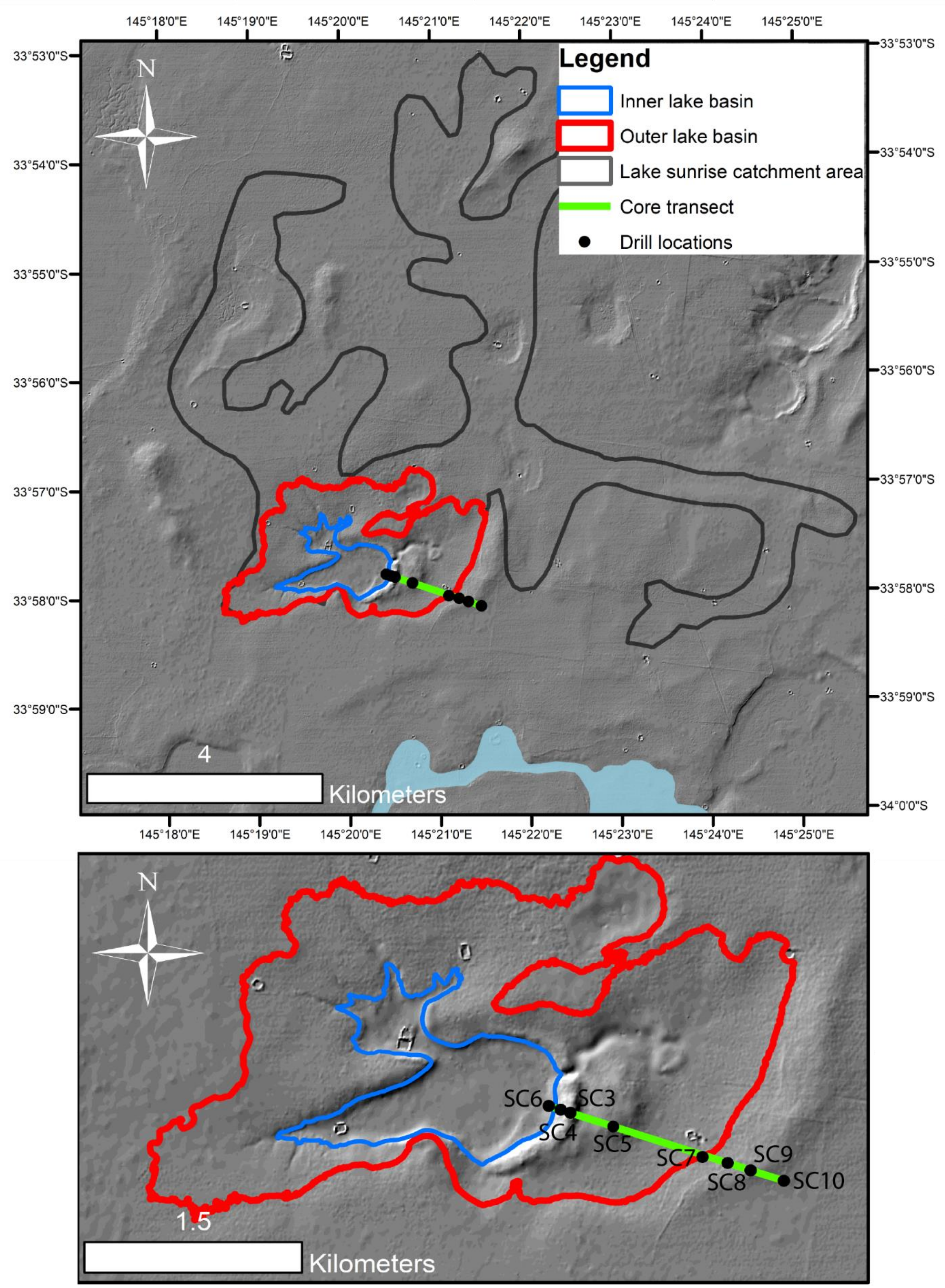

Figure 1.3.4 – Map of Lake Sunrise catchment with inset of the modelled inner, middle and outer lake basins as well as the referenced Murrumbidgee palaeochannel to the south (blue). The red line represents the outer lake basin (7.01 km^2), the blue line the inner lake basin (1.15 km^2) and the white cross hatched area represents the catchment of Lake Sunrise (~ 69 km^2). The green line is the transect from which the cores were taken, the specific cores locations are shown in figure 5.2.1(b), (section 5). NSW 5m DEM (ANZLIC Committee on Survey & Mapping, 2021).

1.4 Methods

1.4.1 Field site and methods

Drilling was performed at 8 locations along a transect which began at the base of the inner lunette and finishes at the furthest extent of the outer lunette. A total of 11 cores were taken; 8 for sedimentological analysis and 3 for OSL analysis. The push tube drilling was performed by Connolly Environmental from Melbourne, Victoria. A Geoprobe 7730DT drilling rig (figure 1.4.1), with a Dual Tube DT32 – push tube 47 mm PVC attachment was used to take the cores. The sedimentology cores were pushed down until refusal. Reaching the clay bed deep below the crests of the lunettes was unachievable.

Figure 1.4.1 – (a) A Geoprobe 7730DT drilling rig, with a Dual Tube DT32 attachment. (b) Example of sediment core.

The OSL cores were taken 2 m away from their related sedimentology cores along the same elevation contour. Three direct push OSL cores, situated on the inner (SC4), middle (SC5), outer lunette (SC7) as well as one stainless steel OSL tube hand core used for the nearby paleochannel (SUN2), all taken within a 1 metre proximity to their associated sediment cores. The 47 mm PVC piping with core catchers was wrapped in 4 layers of black contact to reduce the probability of in-situ bleaching of extracted sediments. The cores were wrapped in black plastic and transported back to the laboratory to be opened. Sampling was completed on 19/10/20 over an 8-hour period. There was approximately 15 mm of rain over a 7-day period prior to sampling according to the landholder. Sampling was cut short by a rapidly approaching rain cell.

1.4.2 Sedimentology methods

Particle size analysis was performed on dry sample at selected intervals along each sediment core, typically at changes to colour, texture and carbonate content to try understand the various sediment populations (and facies) that exist in the Lake Sunrise lunette complex. Unit boundaries were visually identified, following which representative samples from each unit weer taken. Prior to analysis, samples were randomly split down to ~ 200 g of sample. Each sample was subjected to a series of pre-treatments. Samples were firstly treated with 30 % hydrogen peroxide (H_2O_2) for a 24-hour digestion period to remove organic matter. They were then triple rinsed with deionised water and centrifuged, before they were subjected to a 24-hour treatment of 10 % hydrochloric acid (HCl) to remove calcium carbonate, after which they were triple rinsed and centrifuged. Samples were then dispersed using a sodium hexametaphosphate (Na6[(PO3)6]) solution on an end-over-end mixer for 24-hours. Following dispersal, samples were run through a wet splitter to achieve a desirable volume (~ 15 mL) suitable for the

Malvern Mastersizer 2000 laser diffraction particle analyser. The water refractive index was set at 1.333, whilst the particle refractive index was set at 1.544. Samples were exposed to five measurement cycles, during which visual examination of the obscurity and residual of error were observed. The final measurement run was used, as it is generally the most accurate, allowing for the dispersal of particles. The Malvern produces results according to the classification defined by Wentworth (1922) expressed as volume % of the sample.

1.4.3 Dating Methods

All OSL analysis occurred over an 8-month period. Under red light conditions at the Macquarie University Luminescence (TRAPS) laboratory in Sydney, the cores were sliced laterally using a Dremel and split in half, ensuring that the light exposed core endings were removed. Based upon the stratigraphy of the paired sediment cores, the coarsest layers were removed and placed into separate beakers. Three samples from SC4 (230 - 240 cm, 240 – 250 cm, 330 – 340 cm), three samples from SC5 (513 – 516 cm, 550-559 cm, 563 – 566 cm), three samples from SC7 (200 – 220 cm, 236 – 250 cm, 270 – 280 cm) and one sample from SUN2 (~ 100 cm) were targeted. Half of each sample was dried, milled and weighed as a sub-sample for measurements to determine the environmental dose rate. The remaining half was processed in subdued red light; Quartz grains were separated from each sample according to the procedures of Aitken (1998) and treated with 40% hydrofluoric acid for 45 minutes to remove the external alpha-dosed outer layer (Aitkin, 1998). Processed samples were then sieved to separate a target size fraction of 180 – 212 µm. The quartz grains were brushed onto coated 100-hole single grain discs and subsequently loaded onto a 48-position carousel loaded into a Riso TL-DA-20 reader. The reader was fitted with a 10 mW 532 nm Nd:YV04 solid-state diode-pump green laser with 90% power corresponding to 25 W/cm^2, with UV emissions detected with an Electron Tubed Ltd 9235QA photomultiplier tube coupled with a 7.5 mm Hoya U-340 filter. This setup was programmed to stimulate individual Quartz grains at 125ºC for 2 seconds, The single-grain disc locating process was programmed to occur before any disc heating procedure to ensure that each grain received the same heating within the SAR cycles.

Environmental dose rates were estimated through various tests of each milled sample. Beta dose was measured with a Geiger-Muller multi-counter (Botter-Jensen and Mejdahl, 1988), with the attenuation effects of hydrofluoric etching (Bell and Zimmerman, 1978), approximate water content (Aitken, 1998) and grain diameter variation (Brennan, 2003) accounted for in the calculation of the beta dose. Gamma dose rate was estimated from Uranium and Thorium values obtained through thick source alpha counting using a Daybreak 583 intelligent alpha counter (Junding, 1991). The difference between alpha and beta counts from the two counting techniques was used to estimate the potassium values. These values were used to calculate the final gamma dose rate, following the conversion factors of Guerin (2011). Attenuated moisture can have significant effects on the external beta and gamma dose rates (Aitken, 1998), so care was taken to estimate water content values that reflected the change in site hydrology over time. This was estimated by calculating the moisture content of samples in the laboratory, which is representative of their in-situ conditions, and modelling the effects of sample depth and composition over time (see Table x) To account for the influence of cosmic radiation, the relationship between geographic latitude and longitude (-33.58°S, 145.21°E), sediment thickness (in-situ bulk density assumed of 2.0 g/cm^3) and altitude (99 mASL) was used (Prescot and Hutton, 1994).

2 Results

2.1 Sedimentology results

2.1.1 Textural analysis

Sedimentological analysis was performed on 82 samples, spread over 8 cores. Following laser diffraction analysis, the Wentworth sedimentary scale (1922) was used to understand the proportions (%) of clay (< 4 µm), silt (4 – 62.5 µm) and sand (62.5 – 2000 µm) in each sample. As seen in figure 2.1.1, the clay volume in all samples is < 10 %, with the lowest recorded clay proportions present with increasing sand content. Due to the low clay content, there is a clear inverse relationship between silt and sand content, which forms a strong basis for defining textural groups according to the Folk triangle classification of sediments (1954). There are four distinct textural classifications present; the majority of samples can be classified as either 'silty sand' (47.5 %) or 'sandy silt' (43.9%), with two minor classifications present as 'sand' (2.4 %) or 'silt' (6.0 %).

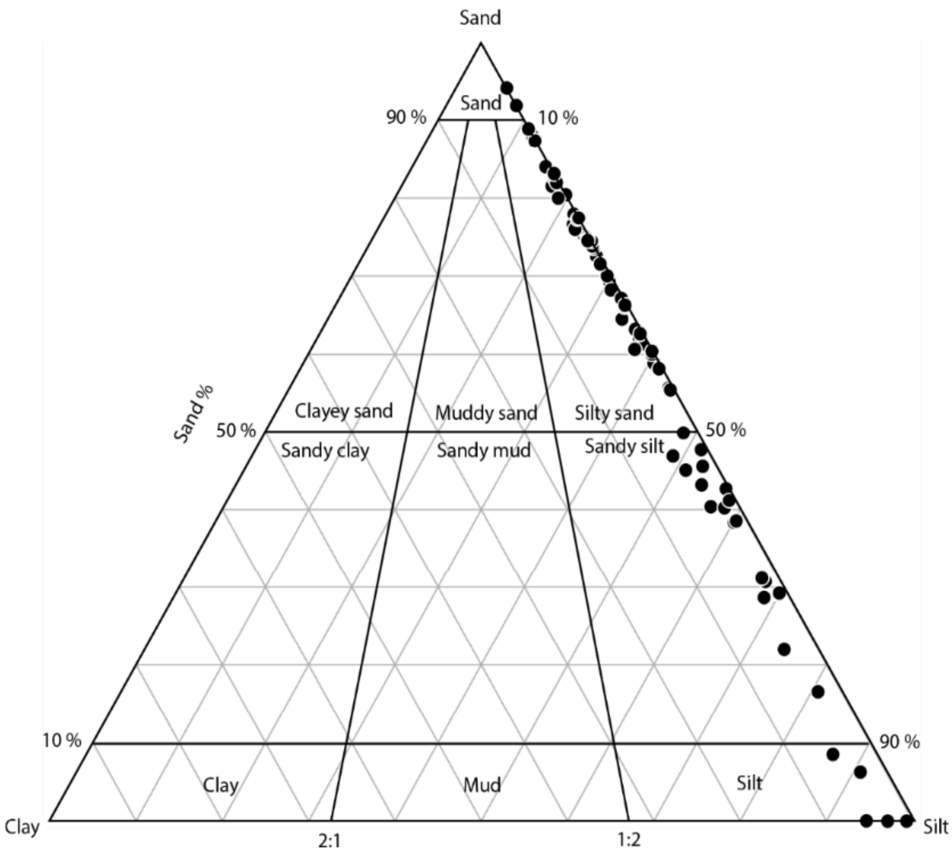

Figure 2.1.1 - Folk classification (1954) ternary diagram showing the proportion (%) of clay, silt and sand for sediment samples at Lake Sunrise. Samples absent of mud content are stacked upon one another in the lower right 'silt category'.

2.2 Modal grain size analysis / sediment facies classification

Following this textural classification, particle size frequency distribution data of each sample were run through a curve fitting program to further understand the modal populations that may be present across the Lake Sunrise basin. The mode, run in excel, iteratively solves for a normal number of distributions which best account of the observed frequency distribution. The modal diameter, standard deviation, and weight (%) of each population are reported. Figures 2.2.1 and 2.2.2 show the curve fitting results from two samples, both representative of the generally trimodal, highly variable sediment populations

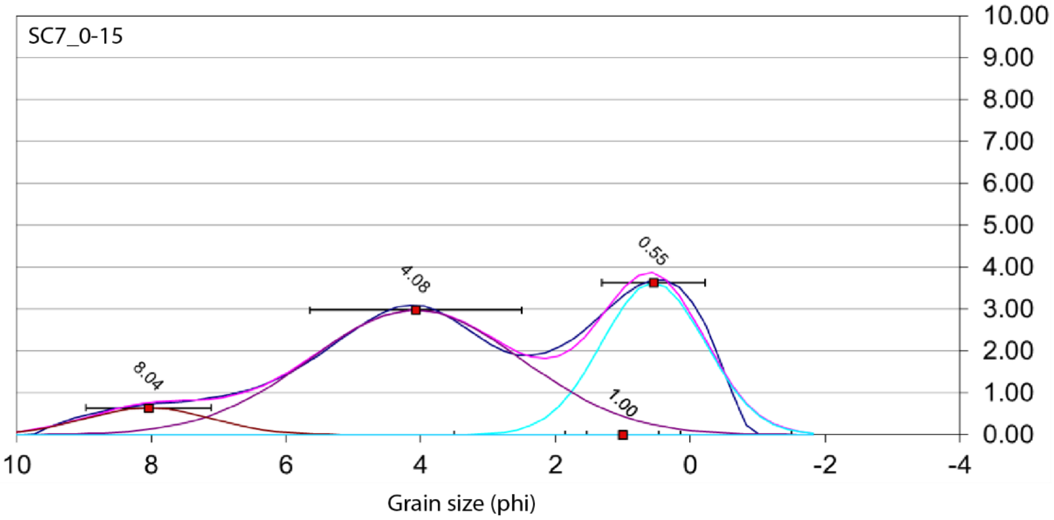

Figure 2.2.1 - Curve fitting graph produced for sample SC7_0-15. The program has identified three significant sediment populations. The most dominant mode occurs at 0.55 phi (coarse sand), with two lesser modes at 4.08 (coarse silt) and 8.04 (clay). The observed frequency distribution is shown in dark blue, the individual populations as brown and cyan and the summed fitted distribution in magenta.

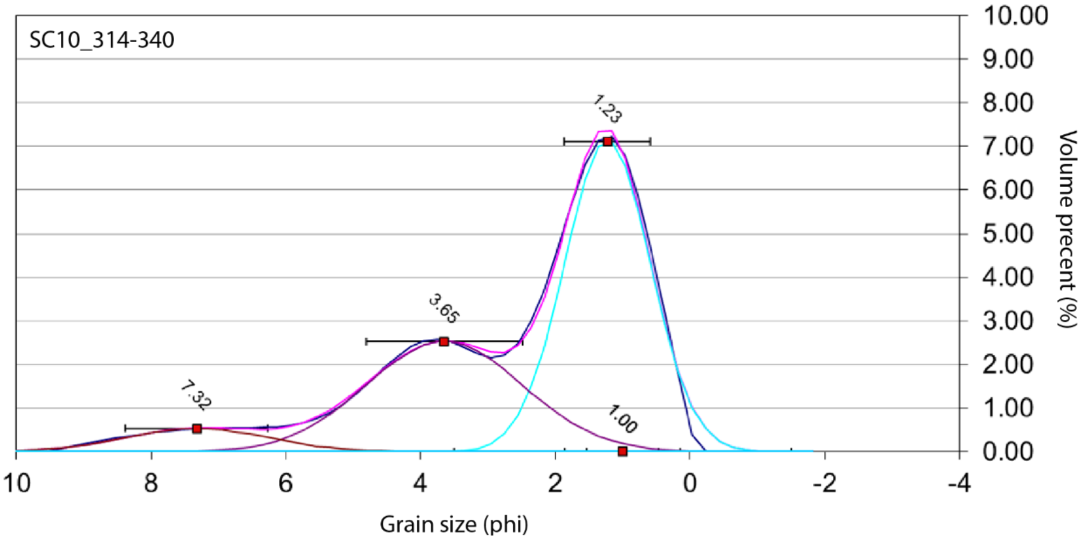

Figure 2.2.2 - Curve fitting graph produced for sample SC10_314-340. The program has identified three significant sediment populations. The most dominant mode occurs at 1.23 phi (medium sand), with two lesser

modes at 3.65 (very fine sand) and 7.32 (fine silt). The observed frequency distribution is show in dark blue, the individual populations as brown and cyan and the summed fitted distribution in magenta.

present across the site. A comparative analysis of the dominant sand fraction mode (62.5 – 2000 µm, < 4 phi) in each sample against the percentage of mud (defined as silt and clay or < 62.5 µm, > 4 phi) was used to probe the depositional environments of these lunette sediments. As seen in figure 2.2.3, there is no clear relationship between mud content (%) and sand size in any of the samples. However, the clustering of modes around 1.5 phi (medium sand) and 3 phi (very fine sand) form strong grounds to create a depositional classification of sediments at Lake Sunrise. Two primary and one secondary depositional regimes exist:

Swash zone deposits (< 2.5 phi) – medium sand representing the coarsest modes deposited via shoreline wave action processes.

Windblown (Aeolian) deposits (2.5 – 4 phi) –Very fine sand populations, deposited through aeolian reworking of shoreline sediments.

Deflated lakebed material (> 4 phi) – Silt and clay sediment populations. Represents fine lakebed sediments reworked by aeolian transport following exposure of the lake floor. These samples are not presented in figure 1.4, as they contain no sand.

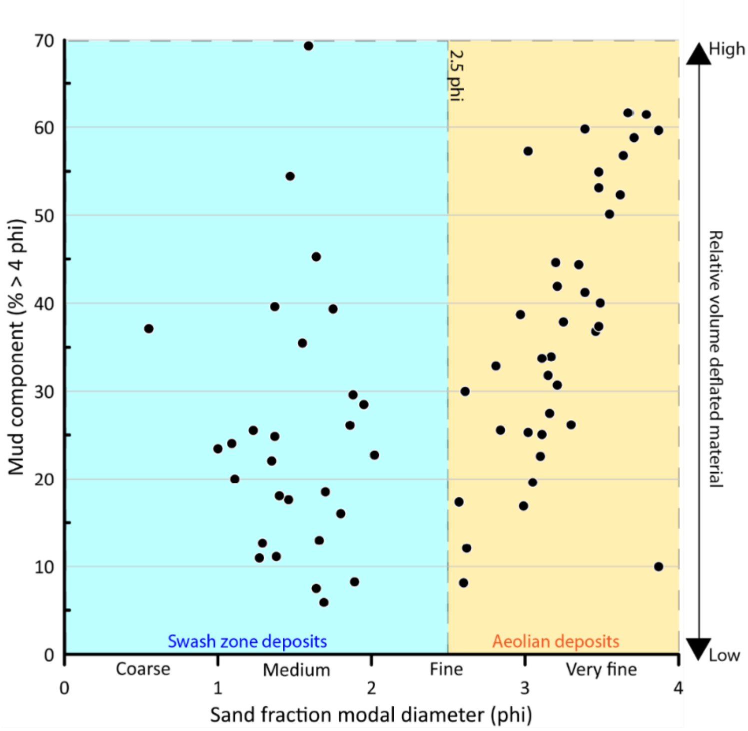

Figure 2.2.3 - Depositional classification of lunette sediment in the Sunrise Lake complex. The Sand fraction modal diameter of each sample is comparatively graphed against mud volume (> 4 phi). Swash zone deposits (< 2.5 phi) and aeolian deposits (2.5 – 4 phi) are clearly defined, with mud material being classed as a secondary depositional population.

There were 66 sandy modes present, ranging from 0.55 – 3.87 phi. 28 (42%) of the samples fell below the 2.5 phi depositional threshold, being classed as 'swash zone deposits. The remaining 38 (58 %) samples fall into the 'aeolian depositional zone', whilst all samples contain a varying volume of secondary deflated material (5.9 – 100 %). Figure 2.2.3 contains sixteen samples with 100% (> 4 phi) mud content and are consequently stacked upon one another, making the visual analysis of totally muddy samples deceptive.

2.3 Core analysis

Three of the eight cores are presented in the following results section and are representative of the sedimentology present across the lunette complex. A core from the inner lunette (SC4), middle lunette (SC5) and outer lunette (SC7) have been chosen, ensuring the three main lunette structures are accounted for (figure 2.3.1).

SC5

Figure 2.3.1 shows the sediment profile for SC5. The core is located at the peak of the middle lunette crest, with a target depth of 580 cm. There are two distinct sediment modes alternating throughout the profile. As seen in the figure, very fine sand dominates almost the entire profile (MD = 3.3 phi), with a small fine sand unit present at 375 cm (2.57 phi). As seen in table 3.1, a light brownish colour consistently dominates the profile, and there is little to no variation in the poorly sorted nature of sediments down the profile. Organics are present in the upper 50 cm, with calcium carbonate and iron concentrates found in the fine sand units throughout the profile. Three samples for OSL were taken from the lower 80 cm of fine sand sand unit. The ages (see section 4) range from 68.5 ± 5.2 ka (bottom) – 50.5 ± 5.5 ka (top).

Table 2.3.1 - Core description table from SC5.

Depth (cm)	Folk classification	Dominant mode (Wentworth scale)	Dominant sand mode (phi)	Sorting	Colour code (Munsell)	Colour
0 - 369	Silty sand	Very fine sand	3.32	Poorly sorted	7.5YR 5/8	
369 - 379	Silty sand	Fine sand	2.57	Poorly sorted	7.5YR 5/8	
379 - 580	Silty sand	Very fine sand	3.39	Poorly sorted	7.5YR 5/8	

SC5

Core SC4 from the inner lunette (figure 2.3.1) is located on the middle of the inner slope of the inner lunette, with a refusal depth of 409 cm. There are four distinct sediment modes alternating throughout the profile. Medium sand is present throughout the majority of the profile (MD [Modal diameter] = 1.52 phi), with the highest proportions occurring at 85 cm, 150 cm, 340 cm, and 380 cm. A single fine sand unit (MD = 2.91) along with three very fine sand (MD = 3.38 phi) and two muddy units (MD = 6.58 phi) intermittently comprise the remaining length of the core. As per table 2.3.2, all units within this core are poorly or very poorly sorted, and there is minimal colour variation down the profile. The presence of iron nodules is concentrated in themlower region of the oxic zone situated within the coarsest units, whilst bands of calcium carbonate sporadically appear throughout the entire core. Organics are present in the upper 50 cm. Three samples for OSL were taken in two of the lower medium sand units. The ages (see section 3) range from 45.1 ± 2.9 ka (bottom) – 24.6 ± 1.4 ka (top).

Table 2.3.2 – Core description table from SC4						
Depth (cm)	Folk classification	Dominant mode	Dominant sand mode (phi)	Sorting	Colour code (Munsell)	Colour
0 - 49	Sandy silt	Very fine sand	3.68	Poorly sorted	7.5YR 5/3	
49 - 123	Silty sand	Medium sand	1.37	Poorly sorted	10YR 7/4	
123 - 147	Silty sand	Very fine sand	3.25	Poorly sorted	10YR 7/4	
147 – 152	Silty sand	Medium sand	1	Very poorly sorted	10YR 7/4	
152 – 164	Silty sand	Fine sand	2.97	Poorly sorted	10YR 7/3	
164 - 219	Sandy silt	Mud	1.59	Very poorly sorted	10YR 7/6	
219 - 290	Silty sand	Medium Sand	1.55	Poorly sorted	10YR 7/6	
290 - 315	Silty sand	Very fine sand	3.21	Poorly sorted	10YR 6/4	
315 – 380	Silty sand	Medium sand	1.8	Poorly sorted	10YR 6/4	
380 – 407	Sandy silt	Mud	1.7	Very poorly sorted	10YR 7/4	

SC7

Core SC7 (figure 2.3.1) is located at the western base of the outer lunette and reaches a depth of 309 cm. There are four distinct sediment modes present in this core. A thin 15 cm coarse sand unit (MD = 0.55 phi) sits at the top of the core, quickly followed by a predominantly muddy unit (MD = 7.59 phi) spanning down to 180 cm. A diffuse transition into a poorly sorted medium sand unit follows (MD = 1.62 phi) reaching a depth of 295 cm before a final very fine sandy unit (MD = 3.87) comprises the remaining length of the core. As seen in table 1.3, there is noticeable colour variation throughout the profile with alternating dark and light brownish hues in the upper 300 cm of the core, followed by a distinct gleyish transition in the lowest unit. All sediments in the profile are poorly/ very poorly sorted. Some organics are present in the upper 40 cm of the profile. Heavy calcium carbonate deposits are found throughout the entire core, with a particular concentration in the muddy unit. Small iron concentrates are found in the mid-section of the medium sand unit. Three samples for OSL were taken in the medium sand unit. The ages (see section 3) range from 90 ± 4 (bottom) to 74 ± 3 ka (top).

Table 2.3.3 – Core description table from SC7.						
Depth (cm)	Folk classification	Dominant mode (Wentworth scale)	Dominant sand mode (phi)	Sorting	Colour code (Munsell)	Colour
0 - 15	Silty sand	Coarse sand	0.55	Very poorly sorted	5YR 5/6	
15 – 180	Sand silt	Mud	7.59	Poorly sorted	7.5YR 8/4	
180 – 295	Silty sand	Medium sand	1.62	Poorly sorted	7.5YR 5/6	
295 - 309	Silty sand	Very fine sand	3.87	Very poorly sorted	2.5Y 7/3	

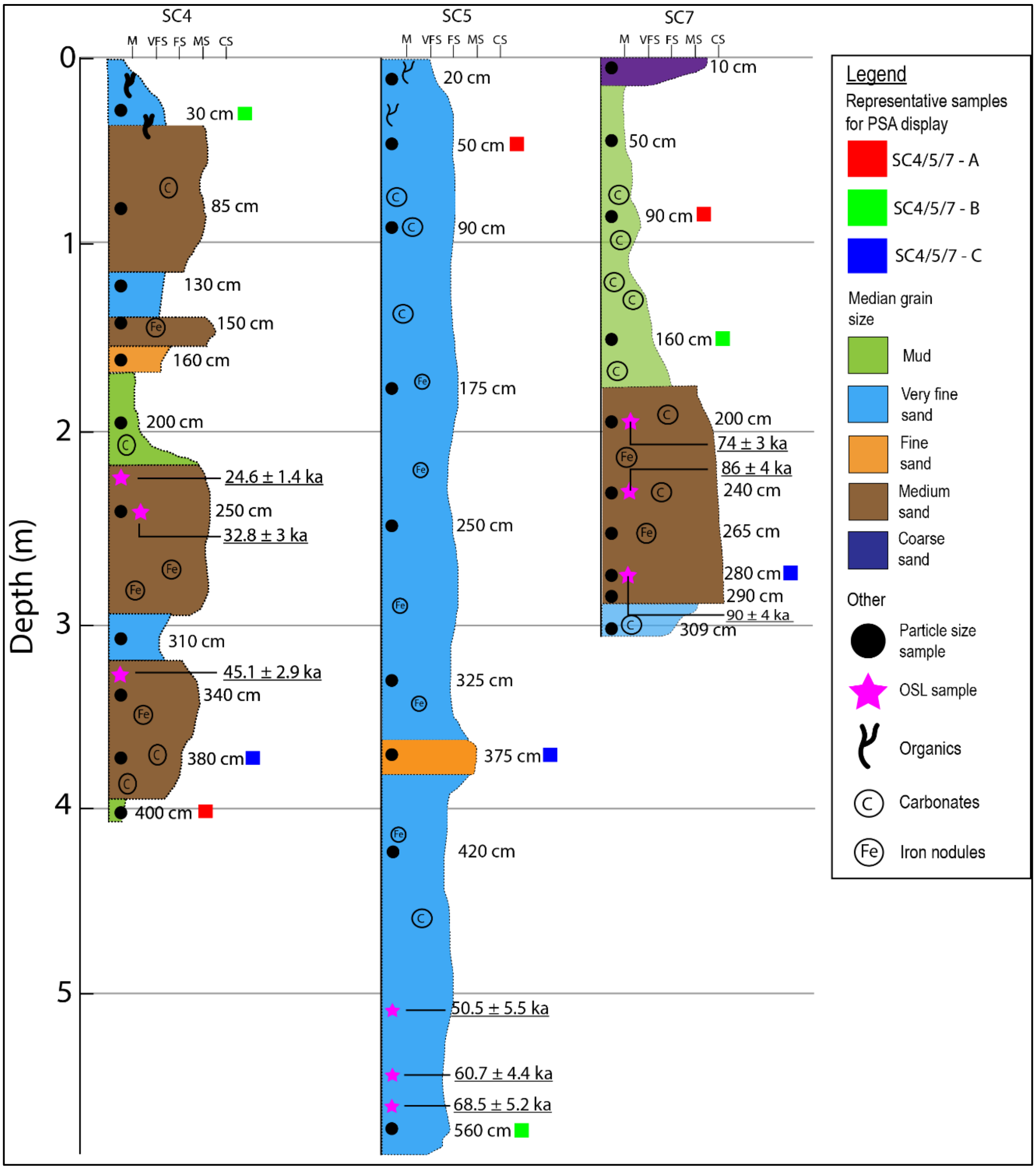

Figure 2.3.1 – Core stratigraphy of SC4,SC5 and SC7 based of PSA and visual analysis. X-axis variations show intra-unit grain size variation, whilst colour represents the median grain size for the entire unit

2.4 Site depositional analysis

By overlaying the sedimentological data presented in the core logs (figures 2.3.1, 2.3.2, 2.3.3) with the three depositional classifications in figure 2.2.3, the differing modes of transport that have contributed to each sample can be better understood.

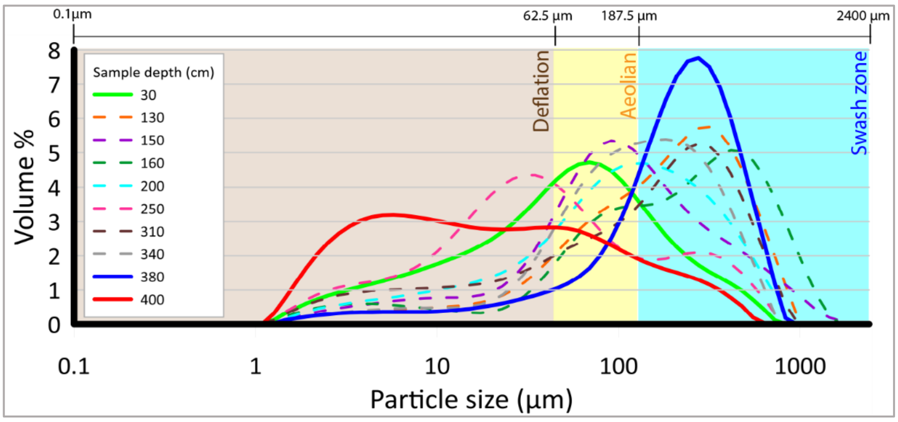

Figure 2.4.1 - Particle size (µm) distribution graph expressed as a volume (%) of samples from SC4.

Ten samples were taken for particle size analysis from core 'SC4' (figure 2.4.1). 70 % of these samples are trimodal in nature, with the remaining 30 % classed as bimodal. The sample from 400 cm contains the finest populations in the core; this trimodal distribution is characterised by a dominant muddy component, as well as two minor components of very fine sand and medium sand. The major depositional mechanism in this sample is deflation, with some aeolian and minimal swash zone influence also occurring. Although all samples in this core have some percentage of influence from deflation, the units at 400 cm and 250 cm are the only samples with > 50 % deflated material by volume. Windborne fine / very fine sand populations are present in all samples, but are most clearly present at 30 cm and 150 cm. Most samples have a significant swash zone depositional component, with 380 cm representing perhaps the cleanest beach swash zone unit in the sample. These results show the sporadic and complex depositional regimes that have contributed to the formation of the

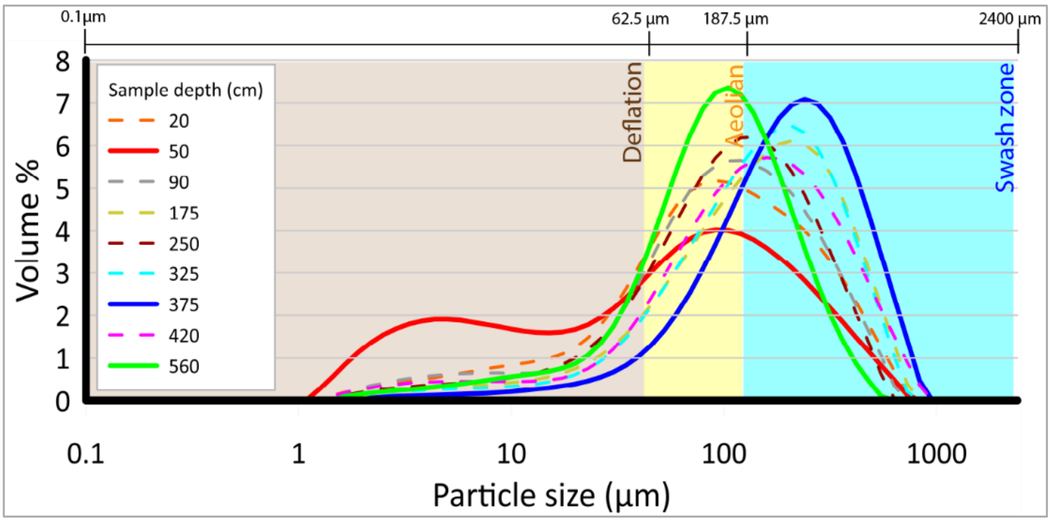

Figure 2.4.2 – Particle size (µm) distribution graph expressed as a volume (%) of samples from SC5.

inner lunette. Ten samples were taken from the crest of the middle lunette 'SC5' (figure 2.4.2). With the exception of 50 cm, having a clear bimodal distribution, the remaining samples have a dominantly unimodal distribution with minor muddy inclusions (< 5%). This finest representative unit, at 50 cm, has a varying degree of aeolian and swash zone influence, as well as a noticeable deflated component. The remaining profile is consistent in particle size distribution, showing a blend of aeolian (represented at 560 cm) and swash zone (375 cm) influence. It can be concluded from these results, the sedimentological composition throughout the SC5 profile (with the exception of 50 cm) have been deposited through the same geomorphic mechanism. In the case of the outer lunette 'SC7' (figure 2.4.3), there is significant variation in the sedimentary profiles of each sample at the site. 50 % of samples have trimodal distributions, as well as bimodal (30 %) and unimodal (20 %) for the remaining samples. At 90 cm, 100% of the sample contains muddy, deflated sediment, in contrast to 280 cm, where almost the entire sample is dominated by swash zone sediments. The relatively low volumes of aeolian material (represented by sample depth 160 cm) suggests that the primary depositional mechanism operating at this point of the outer lunette is swash, however significant muddy inclusions also suggest that deflation also plays a major role in this system.

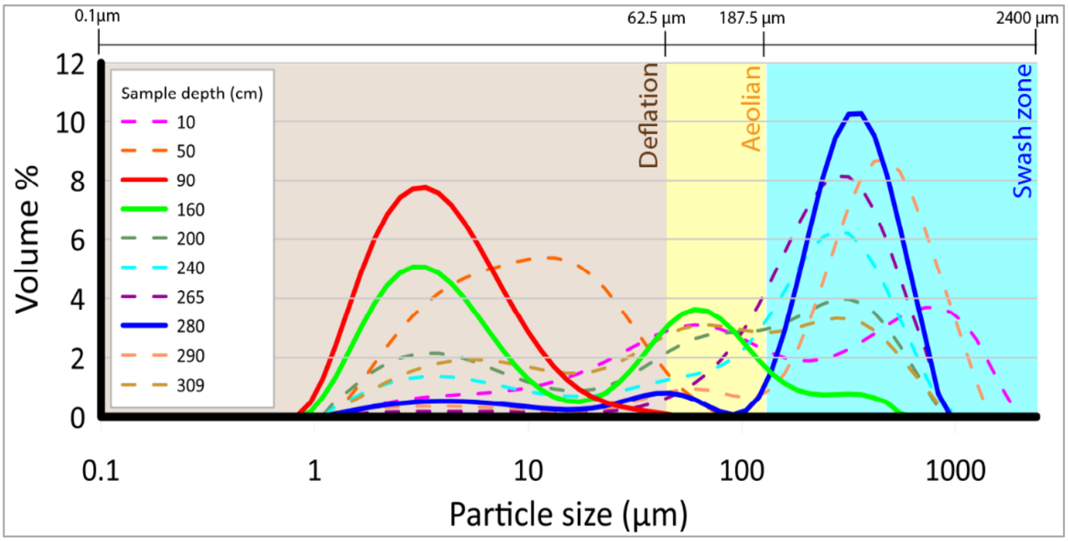

Figure 2.4.3 - Particle size (µm) distribution graph expressed as a volume (%) of samples from SC7.

3. Results – Age Estimation

Optically Stimulated Luminescence (OSL)

Ten single-grain OSL age estimations were obtained from samples collected from three sediment cores on the Sunrise Lake complex. All ten OSL data sets can be found in table 3.1.1, however this results section will focus on three representative samples. Figures for the remaining seven samples, including that from the nearby palaoechannel can be found in appendix 8.2.

3.1 Single-grain quartz D_e distributions

In order to describe the results in detail, three representative samples have been selected. Sampled from the inner (SC4), middle (SC5) and outer (SC7) lunettes, these samples are highly representative of luminescence signal behaviour and consequent results seen in the remaining samples. Intense signal decay is a prominent feature of all samples, decaying by ~ 95% within 0.5s of stimulation (figure 3.1.1). There is wide inter-grain variation in OSL counts (cts) between samples. The youngest samples (SC4) consistently exceed 10,000 cts, having the strongest signal of all samples (maximum signal recorded at 100,000 cts). Samples from the middle (SC5) and outer (SC7) lunettes show greater variability, ranging from 5000 – 30,000 cts, seemingly to the higher dose rates and water content, compared to that of the inner lunette (SC4), see table 3.1.1.There were significant issues with the super-saturation of samples, particularly in those with the most intense OSL decays. Thus, the resulting acceptance rate for grains used in the final equivalent dose determination was low, as most had an 'infinite' equivalent dose. Figure 4.2 shows the estimated dose of samples which were accepted. Following dose testing points at 10 Gy, 20 Gy, 60 Gy, 100 Gy and 200 Gy it was determined that the artificial dosing points for the younger samples (SC4, SUN2) were 20, 60, 100 and 150 Gy, whilst the older samples (SC5, SC7) were 20 Gy, 60 Gy, 100 Gy and 200 Gy, with acknowledgement that the highest doses may approach the upper saturation limits of quartz (Murray and Wintle, 2006). Dose response curves were interpolated to acquire De estimation. The fitting of the dose points on dose response curve is seen in figure 4.2, demonstrating the differences in D_e between samples. The youngest samples are close to the lower dosing point (20 Gy), whilst the older samples sit closer to the upper dosing point (200 Gy).

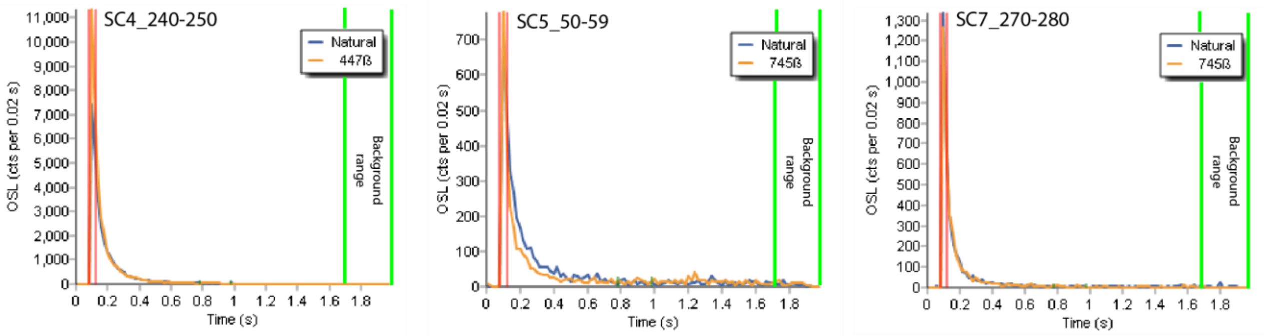

Figure 3.1.1 – OSL decay curves for three samples from the Lake Sunrise lunette complex. Single grain OSL samples from the inner (SC4_240-250), middle (SC5_50-59) and outer (SC7_270-280) lunettes are presented. The decay of OSL counts (counts per 0.02 seconds) is plotted against stimulation duration (seconds). The blue line represents the natural OSL signal, whilst the orange line displays the response of the grain to artificial dose. The green line represents the background signal.

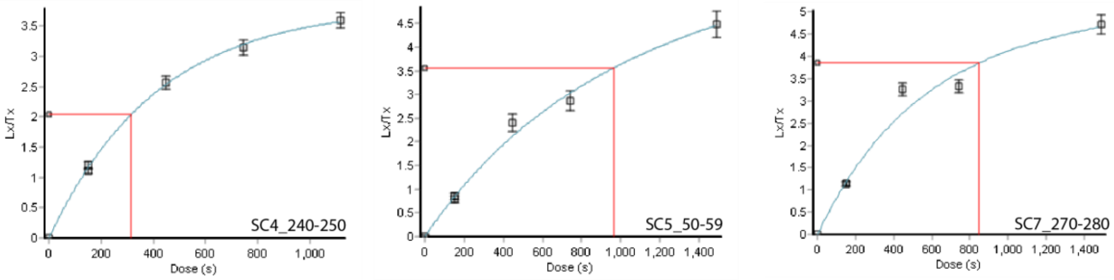

Figure 3.1.2 – Dose response curves for three samples taken from the Lake Sunrise lunette complex. Single grain OSL samples from the inner (SC4_240-250), middle (SC5_50-59) and outer (SC7_270-280) lunettes are presented. The equivalent dose is estimated (red) on the dose response curve (blue). The dosing points are explained in the results section.

Refer to rejections table 3.1.1 for further description of grains exceeding this upper dosing point. Following the analysis of signal decay and dose response, accepted grains were analysed using the Central Age model (CAM) to discern the overdispersion of samples. Overdispersion (%) describes the percentage of grains that fall outside a normal Gaussian distribution. Table 4.1 shows the overdispersion values for all samples. In the case of the youngest samples (SC4), the higher number of accepted grains generates a wider statistical spread of D_e, and consequently a higher number of grains falling outside of a single Gaussian distribution. Plotting these young D_e estimations on radial plots reveals a greater number of highly precise accepted data points falling outside 2 SD error (figure 3.1.3). This is reflected in the relatively high overdispersion value (60%) calculated, suggestive of differences in bleaching or beta dose heterogeneity, discussed in section 4. The middle lunette (SC5) contains grains tightly clustered around the central D_e (figure 3.1.3), even with an overdispersion value (55 %) similar to the youngest samples. This value is skewed as a result of a small number of high precision grains that greatly exceed the 2 SD error. Hence, the overdispersion is not as representative of the true spread of the data. The oldest samples have a significantly lower acceptance rate (4.9 %) compared to the former, as their luminescence characteristics are less desirable than other presented samples. As a result, there is enhanced statistical uncertainty associated with the three SC7 samples, and greater overdispersion observed (72 – 86 %).

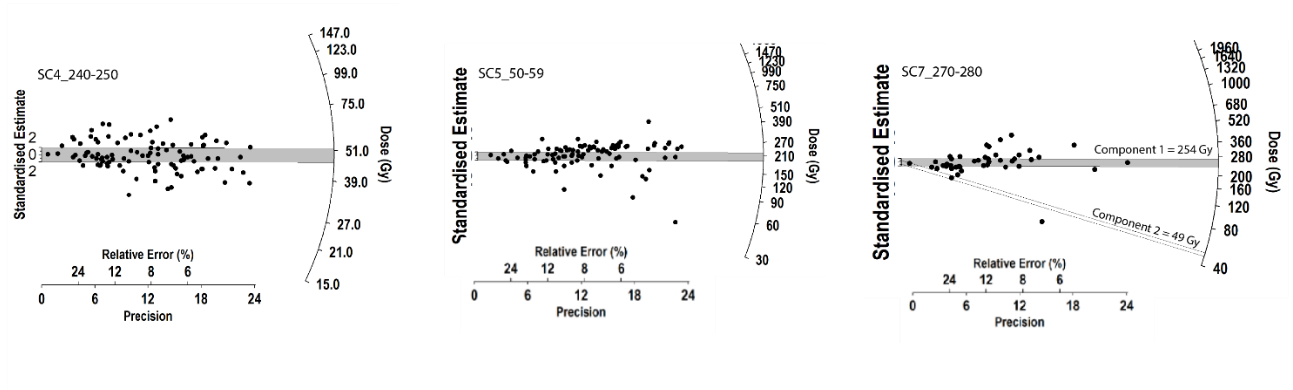

Figure 3.1.3 – Radial plots of OSL samples from SC4, SC5 and SC7 cores, showing the distribution of De from the central De value.

3.2 – Grain screening and rejection criteria

All grains were put through a series of screening procedures (table 3.1.1), to ensure accurate D_e estimations were accepted for use in the final age calculation. Rejections, according to Jacobs et al., (2006) were based on signal strength (< 3 > SD background %), recycling ratios (0.8-1.2) and recuperation (>5 %). Recycling ratios were the most frequently used rejection criteria (38.2 % - 72.4 % of grains), with poor OSL signals a frequent issue with grain dose response (10.8 % - 54.8 % of grains). Recuperation was less so an issue for these samples (4 – 38.5 %). During a final visual analysis of the data, , super saturation of quartz grains was the most significant issue in the oldest samples (25 – 72.3 % of grains). Super saturated grains are those with such a high natural signal that it cannot be recovered in a laboratory setting using artificial dosing. Acceptance rates were lowest for the outer lunette samples (4.8 %), followed by the middle (11.5 %) and inner lunettes (19.8 %). There is an apparent trend of acceptance rates increasing for younger samples.

Table 3.1.1	**Sample ID**		
Rejection criteria	SC7_270-280	SC5_50-59	SC4_240-250
Total Grains	900	600	500
Initial rejection phase*			
Poor signal <3 >sd bg[a] (%)	54.8 %	10.8 %	23.2 %
Recycling ratios > or < 0.8-1.2[b]	56.2 %	38.2 %	72.4 %
Recuperation >5 % [c]	38.5 %	4 %	12.8 %
Grains progressing to final dose response curve analysis	156	260	132
Super saturated [d]	72.3 %	63.1 %	25 %
Accepted grains	43	96	99
Total acceptance rate (%)	**4.8 %**	**11.5 %**	**19.8 %**

* Grains may be rejected on multiple criteria, reflective in the percentage of each rejection category.
[a] Observed natural signal exceeding background standard error (3SE).
[b] Recycling ratio exceeded acceptance range (0.8-1.2).
[c] Zero dose signal greater than natural signal.
[d] Natural signal projected outside of regenerative dose points.

3.3 – Environmental dose rate

The total environmental dose rates are provided in table 3.1.2. The quartz total dose rates in the youngest samples (SC4) range from 1.99– 2.62 Gy/ka, whilst the oldest 6 samples (SC5 and SC7) tend to be much higher, ranging from 2.66– 3.90 Gy/ka. Depth appears to insignificant in this variation, rather, it has an influence on the preservation of moisture content (%), with deeper samples retaining higher volumes of water. The water content values presented in table 4.2 are measured within 7 days of core extraction. They are deemed fairly representative of the water content values that would have been present during the late Quaternary, to be discussed in section 4. Thus, water content, a function of depth, plays a primary role in the variation of environmental dose rates. This can be observed when comparing the water content between middle lunette (SC5) and inner lunette (SC4) samples. The water content values (%) for the middle lunette complex are relatively high, ranging from 14 ± 2 % - 15 ± 2 %, these samples were taken from a 560 cm – 603 cm section of core. In comparison to the much lower 1 ± 1 – 9 ± 2

% observed in the inner lunette, where sample depth ranged from 230 – 300 cm. The contribution of sedimentary composition must also be recognised in the retention of moisture content. Sedimentological analysis from the inner (SC4) and outer lunettes (SC7) highlight the dominantly shoreline or 'swash zone' sediments (medium sands, see figure 2.2.3 section 2) in comparison to the finer aeolian deposits (fine sands). The lower porosity in the finer sediments allows them to retain more moisture and therefore record a higher moisture content.

3.4 Final OSL age estimation

The final OSL age estimates are presented in table 3.1.2. The inner lunette complex (SC4) contains the three youngest ages observed across the site. The ages range from 45.1 ± 2.9 ka - 24.6 ± 1.4, increasing in age with depth. The age estimations in this core are in stratigraphic agreement; they do not overlap in range and have similar environmental dose rates (1.99 0- 2.62 Gy/ka). The transition of ages between the inner and middle lunette sequences do not overlap, as the estimations of all SC5 samples range from 68.5 ± 5.2 - 50.5 ± 5.5 ka. The fluvial sediments of the nearby paleochannel (SUN2) have an estimated age of 46.6 ± 3.9 ka. The age estimations for the outer lunette structure (SC7) are far more complex, ranging from 90.1 ± 3.5 – 74.7 ± 3.4 ka. The combination of low grain acceptance rates and high overdispersion results in individual age ranges ± > 10 % from the central age value. A summary of the overlapping probability of ages occurring around their central value are presented in figure 3.1.4. The greatest probabilistic uncertainty is found in the OSL samples from the middle lunette, overlapping slightly with the probability density curves for the inner and outer lunettes. Justification for the model selection for each sample can be found in section 4.1.

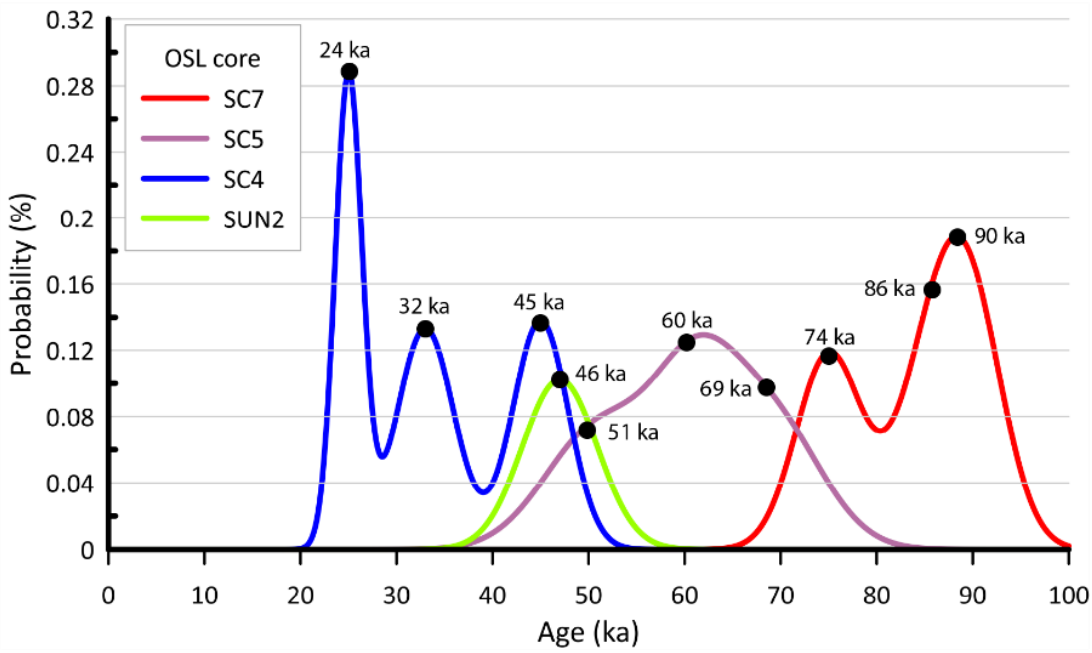

Figure 3.1.4 – Probability density function chart of OSL age estimates from the Sunrise Lake complex. The probability (%) of age estimation (ka ±) is presented. OSL samples from the same cores are graphed on the same-coloured line. The overlapping age ranges are best visualised using this method. Increasing age range with the central age value results in significant overlap of the oldest two sites (SC5, SC7).

Table 3.1.2											
Sample	**Depth (m)**	**Water content (wt.%)[a]**	**Dose rate**				**Burial dose**		**Geomorphic Unit**	**Dating model**	**Age (ka)**
			Beta (Gy/ka)[b]	Gamma (Gy/ka)[c]	Cosmic (Gy/ka)[d]	Total (Gy/ka)	σD %[e]	D_E (Gy)[f]			
SC4_230-240	2.3	0.75 ± 0.3	1.11 ± 0.05	0.65 ± 0.03	0.20 ± 0.02	1.99 ± 0.08	41%	49.0 ± 2.1	Upper swash zone	**CAM**	**24 ± 1**
SC4_240-250	2.4	1.5 ± 0.5	1.35 ± 0.07	0.81 ± 0.04	0.16 ± 0.02	2.35 ± 0.11	60%	77.3 ± 6.1	Upper swash zone	**CAM**	**32 ± 3**
SC4_330-340	3.3	6.75± 2.3	1.52 ± 0.07	0.89 ± 0.04	0.18 ± 0.02	2.62 ± 0.12	39%	118.1 ± 5.5	Upper swash zone	**CAM**	**45 ± 3**
SC5_13-16	5.6	11.25.± 3.8	2.02 ± 0.16	1.75 ± 0.13	0.09 ± 0.02	3.90 ± 0.28	46%	196.7 ± 16.1	Aeolian	**CAM**	**50 ± 6**
SC5_50-59	5.8	10.5 ± 3.5	2.08 ± 0.10	1.24 ± 0.05	0.09 ± 0.01	3.45 ± 0.16	55%	209.2 ± 12.1	Aeolian	**CAM**	**60 ± 4**
SC5_63-66	6.0	10.5 ± 3.5	1.90 ± 0.08	1.19 ± 0.04	0.09 ± 0.01	3.22 ± 0.12	37%	220.5 ± 14.5	Aeolian	**CAM**	**68 ± 5**
SC7_200-220	2.2	4.5 ± 1.5	1.63 ± 0.07	0.84 ± 0.03	0.16 ± 0.02	2.66 ± 0.11	72%	219.1 ± 0.1	Lower swash zone	**FMM**	**74 ± 3**
SC7_236-250	2.4	5.25 ± 1.8	1.81 ± 0.09	0.93 ± 0.05	0.15 ± 0.02	2.93 ± 0.13	86%	239.2 ± 0.1	Lower swash zone	**FMM**	**86 ± 4**
SC7_270-280	2.7	5.25 ± 1.8	1.85 ± 0.09	0.91 ± 0.04	0.15 ± 0.01	2.94 ± 0.13	71%	254 ± 0.1	Lower swash zone	**FMM**	**90 ± 4**
SUN2	1.0	5.25 ± 1.8	1.66 ± 0.10	1.05 ± 0.07	0.18 ± 0.02	2.92 ± 0.17	34%	136.3 ± 7.9	Palaeochannel	**CAM**	**46 ± 4**

a – Water content determined from measurement of wet weighted sample to dry weighted (%) under laboratory conditions.
b – Beta dose rates measured from milled dry sample. Beta count was compared to a standardised beta source (SHAP - 5.99 Gy/ka and MgO – surrogate background value).
c – Gamma dose rate estimated through alpha counting. The Uranium / Thorium from beta dose was used to estimate potassium values, from which gamma dose rate can be calculated (Guerin, 2011).
d – Cosmic date rate estimated using Prescott and Hutton (1994), geographic latitude and longitude (-33.58°S, 145.21°E), sediment thickness (in-situ bulk density assumed of 2.0 g/cm^3) and altitude (99 mASL).
e – Overdispersion (oD%) – percentage value of intrasample statistical spread considering all other variables of sample measurement uncertainty.
f – Equivalent dose (Gy) central value from single grain analysis.
Note – The internal dose rate of all samples was 0.03 ± 0.01 Gy/ ka (Feathers and Miglorini, 2001).

4 – Discussion – Age estimation

4.1 – Age model selection

Central Age Model (CAM)

The central age model (CAM) was used to calculate the age estimations for the inner lunette (SC4), middle lunette (SC5) and palaeochannel (SUN2). The CAM is applied under the assumption that grains are fully bleached before deposition and begin to accumulate 'signal' contemporaneously upon deposition. In theory, the calculated D_e of grains should demonstrate minimal variance from the central D_e value, this variance is represented by the overdispersion (Od %) value (Galbraith et al., 1999). A multi-variate approach, accounting for depositional environment and overdispersion was used as a basis for selecting the central age model for the following samples. It is important to note, that due to issues with super saturation in the majority of grains, that the ages produced from the CAM should be considered as minimum ages, rather than central ages. Thus, they may very well be underestimates of the true age.

Inner lunette – SC4

The three samples used for OSL age estimation from the inner lunette (SC4) were taken from similar sedimentological units. These units are classified as 'swash zone' deposits based on their sedimentary characteristics, as presented in section 2 (figure 2.2.3). Poorly sorted, medium sands dominate these units, and are directly overlain by fine aeolian sand. As seen in figure 4.1.1, the core is located in a zone of the active beach front known as the 'wave run up limit', or the greatest vertical extent at which grains will be deposited under 'swash zone' action (Nielsen and Hanslow, 1991). The thin splays of sediment in the upper most regions of the swash zone provide optimal conditions for enhanced cosmic radiation exposure and signal resetting, whilst the low post-depositional mixing rates, a function of reduced wave energy (Sherman et al., 1994) and topographic position (figure 4.1.1) also provide strong grounds for the assumption of homogenously deposited, well bleached grains. The grains in this zone are continuously turned over in the shallow water, but do not extensively mix with underlaying sediments. Depositional depth also plays a significant role, as primary bleaching occurs more effectively in sediments closer to the mean water surface level (Cunningham et al., 2014). In this upper swash zone, the very poor sorting of thinly deposited sediments is the primary mechanism behind the high overdispersion. Fuchs and Lomax (2019) explain that there are intrinsic differences in dose delivery between fine and coarse grains within an aliquot, with finer grains showing lower variations in D_e compared to coarser grains. Given the mix between grain sizes in this sample, and its distinct position in the shallow regions of the swash zone that allow for optimal cosmic exposure (and homogeneous bleaching), the CAM is the most logical age model to apply.

Middle lunette – SC5

The three samples used for OSL age estimation from the middle lunette are all aeolian in nature, residing within a continuous deposit of a predominantly very fine sand sheet. Following the facies classification presented in section 2 (figure 2.2.3), this sediment has been blown from the beach face and redeposited as dune sediment, forming the crescentic aeolian structure referred to as a lunette. Thus, the aeolian reactivation of this sediment provides the preferable conditions for enhanced cosmic radiation exposure and significant signal resetting. The overdispersion values from these samples (37 % – 55 %) is slightly higher than the earliest reworked dune sediments of Lake Mungo (Jankowski et al., 2020), where overdispersion values ranged from 23 % - 46 % and were deemed acceptable for central age modelling following sedimentological analysis. Beta dose heterogeneity is largely to blame for the high overdispersion values in the aeolian SC5 OSL samples. Clusters of heavy minerals deposited with the quartz grains have likely led to the heterogeneous beta dose attenuation in this sample, particularly in these samples, which were visibly rich in K-feldspars and zircons. This relationship is well documented (Cunningham et al., 2012) and is a strong means of explaining the overdispersion of SC5 samples.

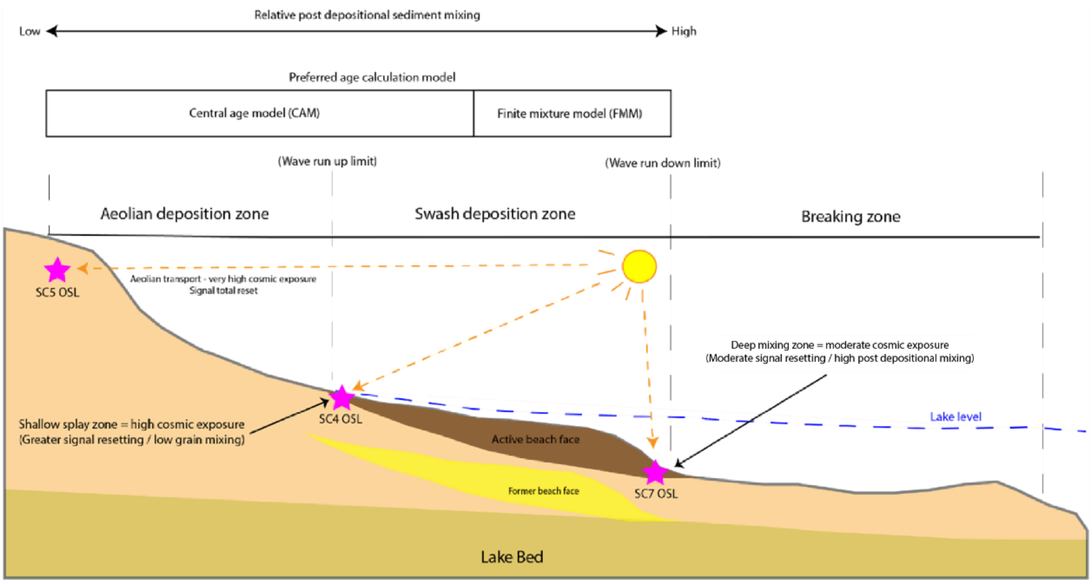

Figure 4.1.1 – Cross section of lake beach dynamics and their influences on OSL signal resetting, post sediment mixing and age model selection. Pink stars indicate where samples were taken for this study, whilst the blue dotted line represents the lake level at the time of deposition. Note the wave run up and wave run down limits being the two most critical zones for differentiating the perceived amount of bleaching pre deposition. Diagram is not the scale.

Palaeochannel – SUN2

The nearby palaeochannel was included as a proximal but disconnected regional indicator of hydrological activity. This fluvial sediment is located 65 cm below the surface, observed in the field as a well sorted medium-coarse sand with indiscernible mud. The sample was likely from the upper ridges of a convex bank scroll bar. The relatively low overdispersion (34 %) can be explained by a well-developed clay capping immediately over the sandy and pedogenesis introducing iron coatings on grains, as was observed in the field. This effect can lead to differences in beta dose heterogeneity (Lomax et al., 2007).

Finite mixture model (FMM)

The finite mixture model (FMM) is best suited to OSL samples where post-depositional mixing of grains is suspected. The FMM identifies multiple D_e populations or ‘components’, their respective doses and the proportion of these varying components within a sample and is well documented in the literature as an effective means of accounting for post-depositional mixing of well bleached grains (Bateman et al., 2007; Jacobs et al., 2008).

Outer lunette – SC7

Grains from the outer lunette appear to have experienced some form of post-depositional mixing. The very poorly sorted, medium - coarse unit that the OSL samples have been taken from resides in the wave run down limit or 'deep mixing zone', as seen in figure 4.1.1. Being located on the wave run down limit ensuring that grains are still exposed to sufficient cosmic radiation to be fully bleached before deposition, however it also means that these well-bleached grains are more susceptible to post depositional mixing as evidenced by the two populations in each sample with different central D_e values or 'components'. The high overdispersion values (71 % - 86 %) agree with this assumption (Thomsen et al., 2012) and support the application of the FMM. Two components were present in all three outer lunette samples, as seen in table 4.1.1. The highest proportion component, in this case, with the highest equivalent dose (De) for each sample was used as the De for age calculation.

Table 4.1.1				
Sample ID	Component 1 (De)	Component 1 %	Component 2 (De)	Component 2 (%)
SC7_200-220	239.16	81.87 %	42.47	18.13
SC7_236-250	219.02	92.17 %	16.88	7.83 %
SC7_270-280	254.29	94.23 %	42 .92	5.77 %

4.2 - OSL age vs depth modelling

Figure 4.2.1 shows the projected age of sediments throughout cores SC4, SC5 and SC7 based on the actual OSLage (ka) estimations and depth (cm). For core SC4, a smoothing spline function was used to estimate the age – depth function up until the present. For this core, the presented model is highly speculative as it assumes the continuous accumulation of sediment up until the present day at more or less the same rate. This highlights the need for further OSL dating higher up the core. Nonetheless, from this age model the two upper (undated) swash zones are modelled to have been active between 11 – 9 ka and 7 – 2 ka into late MIS1. For the aeolian sediments of the middle lunette (SC5), the model assumes that accumulation ceases contemporaneously with the activation of the inner lunette (~ 45 ka). Interestingly, there is an apparent acceleration of dune accumulation from 2.5 cm / 1000 years (70 – 50 ka) to 110 cm / 1000 years (50 – 45 ka), likely as lake levels receded from 'high' to 'moderate', exposing a greater volume of upper swash zone fines to aeolian reactivation. However it could also be speculated that the uppermost sediments of the middle lunette may be blown over from the inner lunette. The acceleration of dune accumulation also occured in the outer lunette samples (SC7), highlighting the varying accumulation rates experienced in the swash zone (4.8 cm / 1000 years) in comparison to the accumulation of deflated fines 53 cm / 1000 years. This difference in rates is likely due to the continual reworking of swash zone sediments, similar to that observed in fluvial sediments of the Murrumbidgee (Mueller et al., 2018). This inference strengthens the explanation of the high overdispersion values in the outer lunette samples (table 3.1.2).

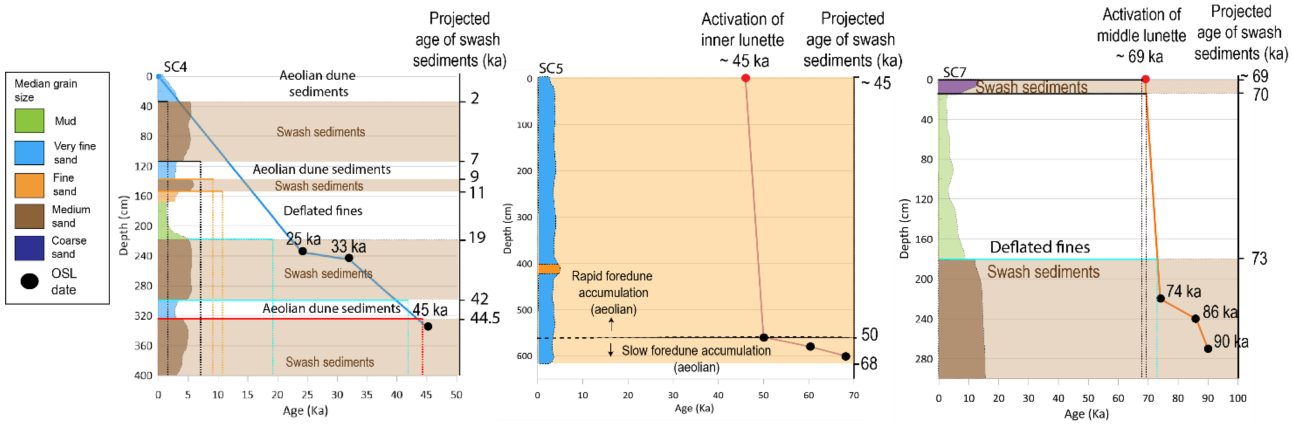

Figure 4.2.1 – OSL age vs depth models with accompanying core logs. The median grain size is differentiated using colour (refer to legend), whilst the brown and yellow shaded regions represent swash zone and foredune deposits respectively, as detailed in figure (2.2.3). Age estimation is derived off the main regression lines through each model.

4.3 – Water content estimation

. The water content values from the Lake Sunrise lunette complex play a significant role in the environmental dose rate calculation. The long term (late Quaternary) water content values (%)) have been estimated using a multi-factorial approach, taking into account observed water content, depth and sediment composition, as seen in table 4.2.1. The model attempts to estimate the rate at which moisture may attenuate as a function of depth, as the locations where the OSL samples were taken all would have been alternately saturated and dried as the water table fluctuated throughout the Quaternary, it can be assumed that the rate at which they were exposed to moisture was uniform across the entire site. Water tends to accumulate deeper in the profile, as the compactness of sediment and accumulation of fines increases with depth (Jackson, 2008). By dividing the observed moisture content (%) with the depth of the sample, a generalised moisture content %/ metre rate was calculated for each sample. This was then used to infer the moisture content of a sample at half of its present depth, when it would have been closer to the surface and held less water. The central water content value was simply the halfway point between the modern-day moisture content and water content at 50% depth. To account for the variability in soil matrix, noting that finer sediments such as silts and clays retain moisture more effectively than sand (Breitner et al., 2010; Rozenweig and Porat, 2015), a 'contributing porosity factor' was estimated and applied to the final error calculation. This novel approach retains continuity between all samples but attempts to account for long term water content, which is a common unknown with OSL environmental dose rate estimations.

Table 4.3.1 - water content estimation table based off depth, sedimentology and observed water depth.										
Sample ID	**Depth (m)**	**[a]W_O (%)**	**[b]$W_{\%}$/m**	**[c]$W_{\%}$/ 50 % depth (m)**	**[d]Central Wc $_{\%}$ value**	**[e]Error (50% central value)**	**Sediment type**	**[f]Contributing porosity factor**	**Final error (%)**	**Actual water content**
SC4_230-240	2.3	1 ± 1	1.15	0.5	0.75	0.25	Medium sand	1.015	0.3	0.75 ± 0.3
SC4_240-250	2.4	2 ± 1	1.2	1	1.5	0.5	Medium sand	1.015	0.5	1.5 ± 0.5
SC4_330-340	3.3	9 ± 2	1.65	4.5	6.75	2.25	Medium sand	1.015	2.3	6.75± 2.3
SC5_13-16	5.6	15 ± 2	2.8	7.5	11.25	3.75	Very fine sand	1.0115	3.8	11.25 ± 3.8
SC5_50-59	5.8	14 ± 2	2.9	7	10.5	3.5	Very fine sand	1.0115	3.5	10.5 ± 3.5
SC5_63-66	6	14 ± 1	3	7	10.5	3.5	Very fine sand	1.0115	3.5	10.5 ± 3.5
SC7_200-220	2.2	6 ± 1	1.1	3	4.5	1.5	Medium sand	1.015	1.5	4.5 ± 1.5
SC7_236-250	2.4	7 ± 2	1.2	3.5	5.25	1.75	Medium sand	1.015	1.8	5.25 ± 1.8
SC7_270-280	2.7	7 ± 2	1.35	3.5	5.25	1.75	Medium sand	1.015	1.8	5.25 ± 1.8
SUN2	1	7 ± 3	0.5	3.5	5.25	1.75	Coarse sand	1.02	1.8	5.25 ± 1.8

[a]W_O (%) = Observed water content % in situ. [b]$W_{\%}$/m = Observed water content / sample depth. [c]$W_{\%}$/ 50 % depth (m) = Predicted water content at 50 % of original sample depth. [d]Central Wc $_{\%}$ value = Water content value between observed and 50 % sample depth. [e]Allowed error margin = 50% of central W_C % value. [f]Contributing porosity factor = % factor to take into consideration the effects of sediment type on porosity (water retention).

5. Discussion – Paleoenvironmental reconstruction of the Lake Sunrise Basin

5.1 – Classification of sediment facies

The classification of sediment facies is a pivotal process in paleoenvironmental reconstructions. The geomorphic forms, sedimentology and facies of a site enable a unique investigation into the nature and timing of environmental change. Advances in the technologies used to understand these lines of evidence are monumental. From the days of physical cartography, sieves and TL-dating to the now intricately detailed remote sensing, laser diffraction particle size analysis and OSL analysis, a unique opportunity to seek greater detail and understanding of the true sedimentological nature of Quaternary landforms arises.

In this study, facies attribution has relied on particle size analysis in the absence of preserved sediment structures. Various scales have been adopted in the literature, from the early works of Orth (1875), where simple wet sieving into 6 size fractions was sufficient, through to the evolving classifications presented by Atterberg (1911), Doeglas (1968) and more recently Blott and Pye (2012). Udden (1914) and Wentworth (1922) set the basis for defining sediment class boundaries to the present day and are accepted as a reliable and universal means of classifying sediment sizes.

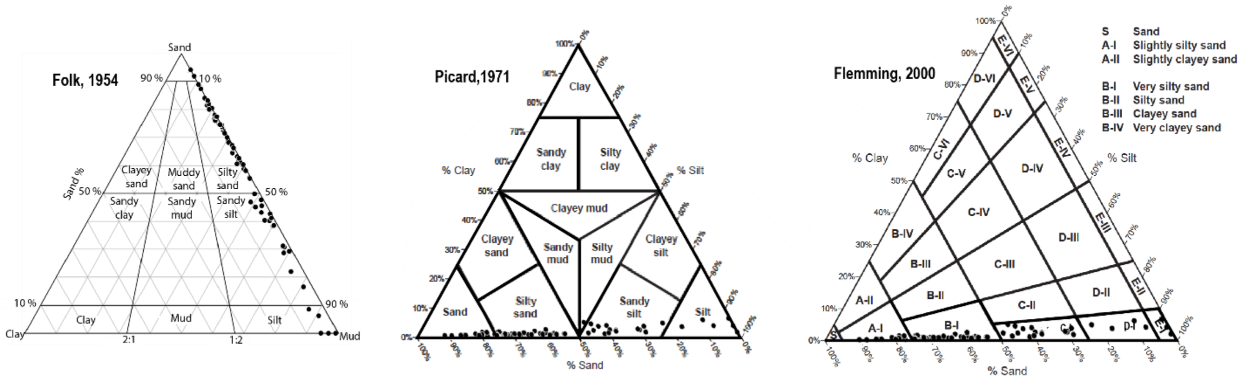

Figure 5.1.1 – Ternary chart comparison using particle size samples from the Lake Sunrise basin. Folk (1954), Picard (1971) and Flemming (2000) ternary classifications have been used, all with different percentage boundaries from differing particles sizes. The resulting sample classifications vary, with a higher proportion of 'sand' in the Picard classification but lower proportion of 'sand' in the Flemming classification when compared to the adopted Folk classification.

The categorisation of particle size (e.g., coarse sand, medium sand, fine sand) is then used as a springboard into a deeper, more quantitative classification, by which varying proportions of different grains in a sample can be easily grouped. Ternary charts provide the simplest way to classify sediments based on the relative percentages of different grain size classes within a sample. Figure 5.1.1 demonstrates the different ways in which these classification schemes (and accompanying ternary charts) classify sediments from Lake Sunrise. Such classifications of sediments according to three coarse size-range fractions do not incorporate the wealth of information available from high resolution particle size distributions (PSD), do not distinguish possibly vital differences within each class, and possibly artificially split natural grain populations at class boundaries.

In an attempt to reduce the inherent complications of using fixed descriptive classification systems, this thesis directly interprets the numerous sedimentary populations in a single depositional unit, groups similar populations between units together and classifies them based on their depositional environment (facies). In the Lake Sunrise basin, three depositional processes (facies) were identified (figure 2.2.3, section 2). These processes have been identified as 'swash zone', 'aeolian saltation' (foredune) and 'deflation' (aeolian suspension and/or fine aggregates). The 'swash zone' is the region of wave break on the foreshore (Stanica and Ungueranu, 2010), and can vary in grade, width and shape (Friedman *et al.,* 1992). 'Swash zone sediments' are a grouping of generally coarse grains, that are mechanically deposited through wave action due to their relatively large size and higher mass (Stanica and Ungueranu, 2010). Studies from the remnant shorelines of Lake George, Australia (Jankowski et al., 2021) corroborate these findings, as a dominantly medium to coarse sand (200 – 2000 um) comprises the beach face and shoreline sedimentary units. Defining an aeolian saltation transport boundary is more complex. This mode of transport relies on a range of variables such as grain mass (mean diameter (um), density (g/cm^3)) and environmental variables (wind direction, wind speed, sediment supply, moisture content). Field and Pelletier (2018) construe the grain-size dependence of aeolian saltation sediments as a primary function of shear surface velocity, whereby 'fine' grains (125 um – 250 um) are increasingly displaced from the beach face towards or parallel to the foredunes as shear velocity increases. Furthermore, similar investigations such as Swann (et al., 2013) demonstrate the preferential aeolian reworking of beach front sediments in the 160 – 170 um size range, whilst Van Der Wal (1998) shows that peak aeolian transport in a dry sediment matrix occurs at 2.5 - 3 phi (125 um – 187.5 um). These approximate boundaries agree with the sedimentological analysis from the Lake Sunrise cores. Figure 2.2.3 (section 2) shows two distinct clusters of modal diameters of grain populations around 1.5 phi (375 um) and 3.5 phi (125 um), with a distinctive boundary between the two clusters such that a boundary can be drawn at ~ 187.5 um. Thus, in this lake system, swash zone sediments are determined to have modal diameters > 187.5 um, foredune sediments between 187.5 um and 62.5 um and secondary deflated sediments < 62.5 um. The relative volume of these differing facies is presented in figure 5.1.2 and is used as a reference for reconstructing the hydrological history of the Lake Sunrise basin.

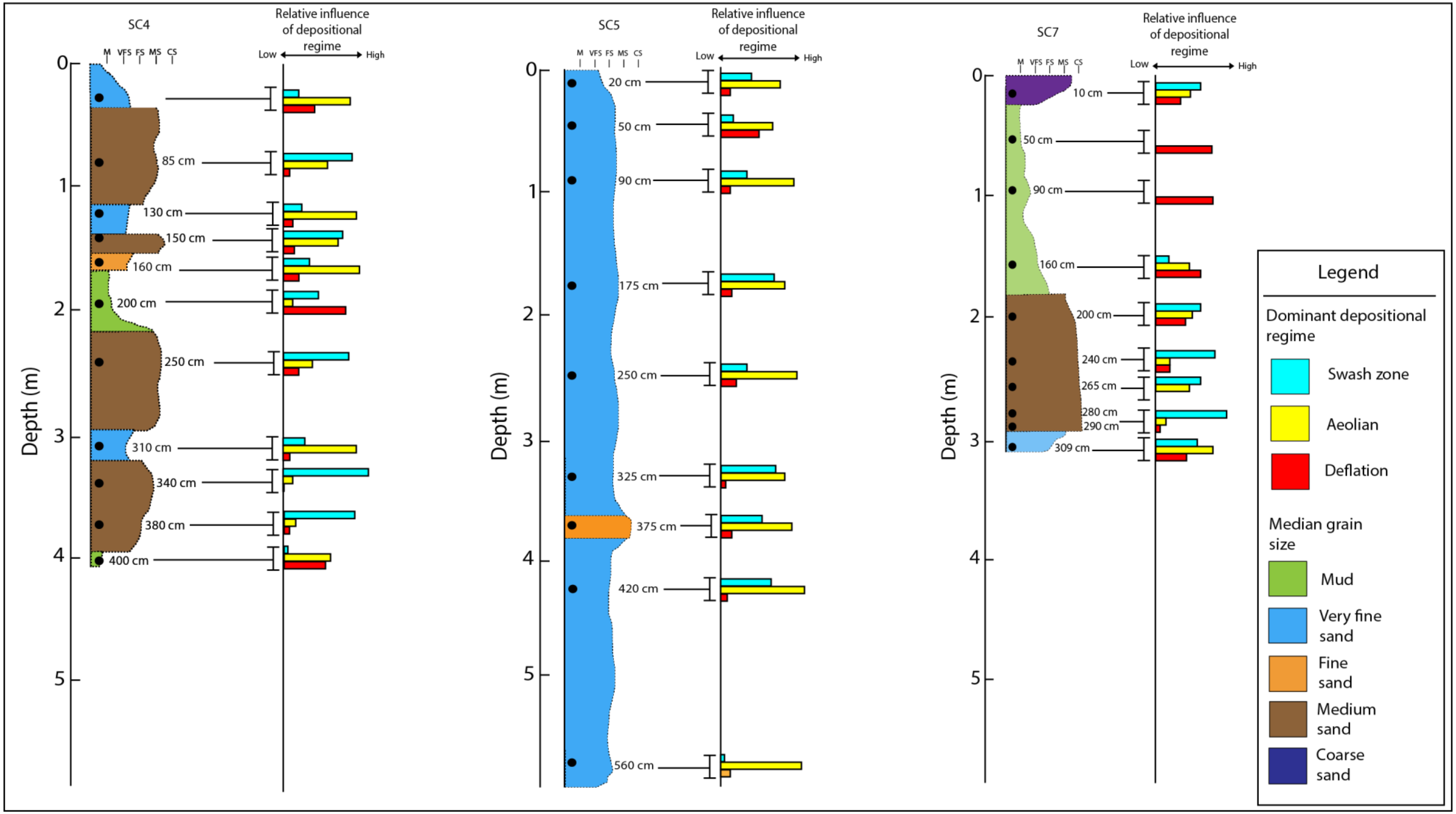

Figure 5.1.2 – Core logs from the inner (SC4), middle (SC5) and outer (SC7) lunettes. The black dots represent the sample locations along the core, whilst the colours indicate the median grain size in each observed unit. The relative proportions of the three depositional regimes for each sample taken in the Lake Sunrise basin are displayed next to each sample within the cores, based on the curve fitting modal analysis (figure 2.2.3, section 2). The relative proportions of swash zone sediments (cyan), aeolian sediments (bright yellow) and deflated sediments (red) are presented.

5.2 – Lake formation and chronostratigraphy

There are ten distinct formation phases in the Lake Sunrise basin. Ascending with age (J = youngest, A = oldest), the phases identified represent changes to stratigraphy, depositional mechanism and hydrological regime; a summary of this is presented at the end of section 5.2 in table 5.2.1. This section will discuss the sedimentology, geomorphology, and age of each phase individually.

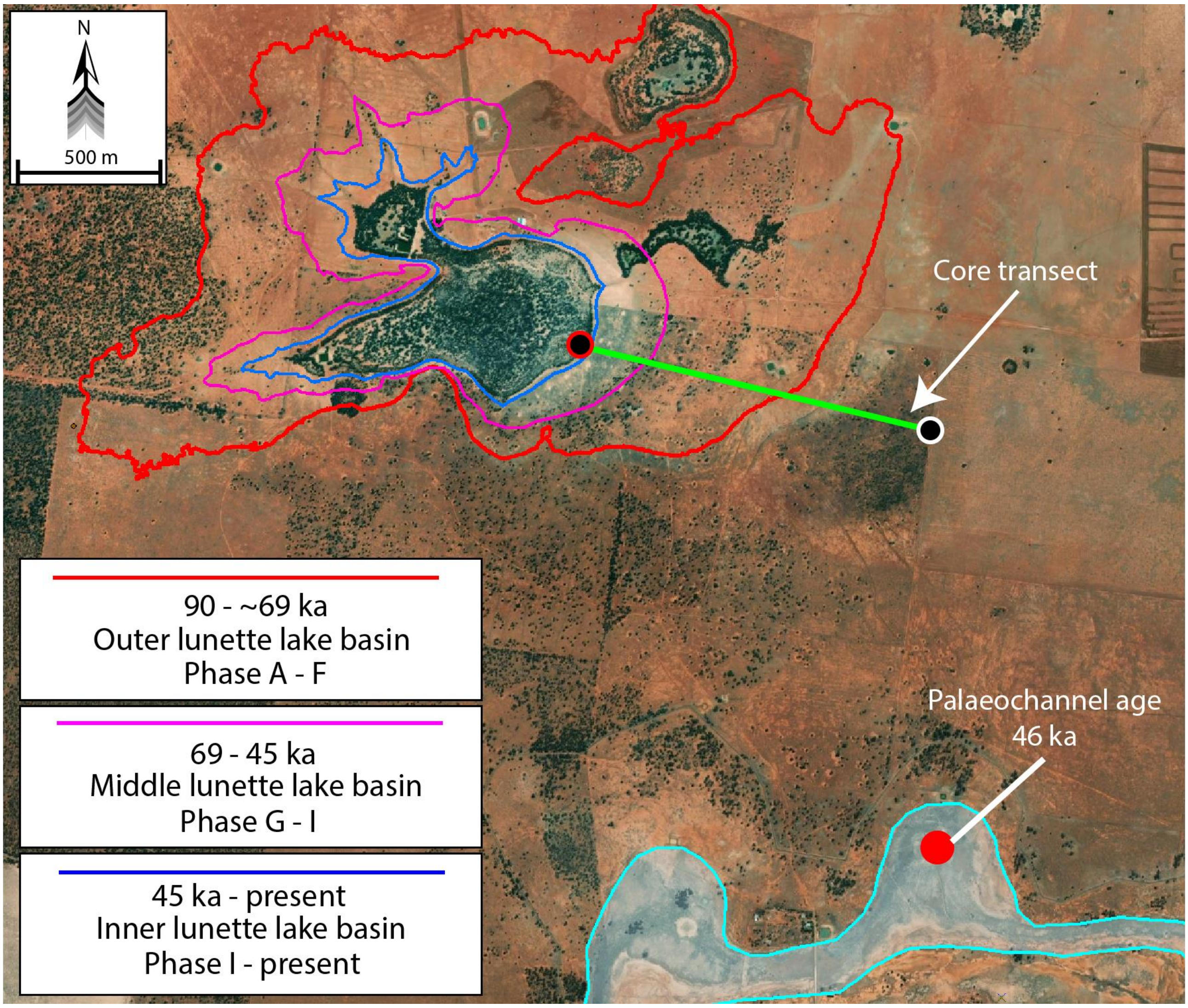

Figure 5.2.1(a) - Lake Sunrise map showing the lake extent during each identified phase. The core transect (green) can be directly paired with the phase diagram in figure 5.2.1(b). The nearby palaeochannel, although completely disconnected from the Lake Sunrise system, has an estimated age of 46 ka., occurring contemporaneously with the inner lake basin (Phase I – present).

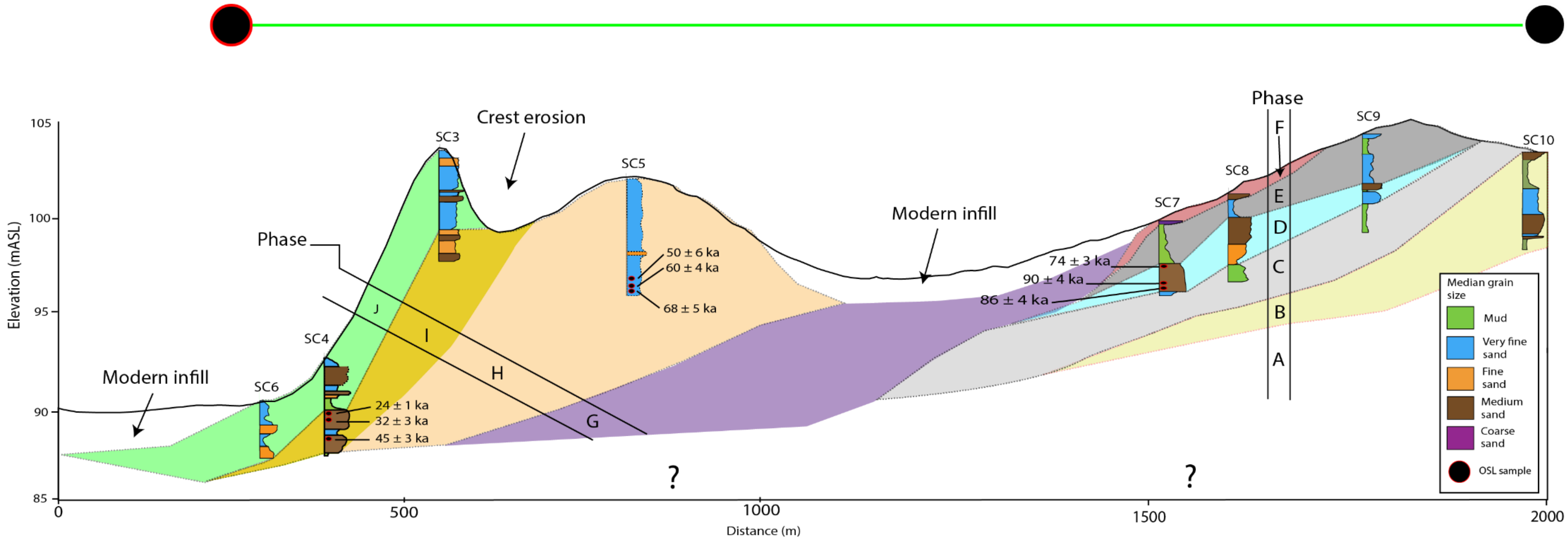

Figure 5.2.1(b) - Lake Sunrise chronostratigraphic schematic cross section showing the location of each sediment core along the lunette complex.. This section shows the cores which display median grain size down with depth and OSL sample location, represented by the colours seen in the legend (bottom right). The phases, also split into colours, represent the sedimentary units that may not necessarily share median grain size, rather, have been deposited over similar temporal periods, and are intrinsically connected through geomorphic processes. A discussion of these respective phases can be found in section 5.2

Chronology of lake formation

5.2.1 - Phase analysis

Phase A: > 90 ka

This phase represents the largely unknown origins of the Lake Sunrise basin. There are two probable explanations for what may be underneath, keeping in mind the cores did not extend into the sediments of this phase. The first explanation is that there may be one or more remnant lunettes, Pleistocene in age, buried deep beneath the surface. The second possibility follows on from the observations by Douglas (1996) at Lake Mungo, whereby it is believed that the Willandra Lakes system was incepted in an ancient fluvial network. A 58.5 m thick (~ 60 m deep) unit of sandy gravel in the nearby Lake Gunbar may be evidence of ancient lacustrine systems existing in the local area (Water NSW, 2021). Surficial evidence of any ancient fluvial systems flowing into Lake Sunrise is lacking, yet flow path analysis using digital elevation models show the likelihood of a chain of lakes, including Lake Sunrise, flowing in a NE to SW aspect.

Phase B: > 90 ka

Phase B is the oldest analysed phase in this study, based on the reconstructed stratigraphy of the outer lunette (Fig 5.2.1(b)), containing an assemblage of stacked lunette sediments that are undated. Phase B can be divided into an upper and lower sequence, related to the depositional regimes under which they have formed. The lower unit shifts rapidly in colour, transitioning from blotchy grey/ red into a golden / yellow massive unit. Very fine sand, aeolian in origin, comprises the mid length of the lower Phase B unit. This unit has noticeable amounts of Fe – Mn concentrates, as well as redox depletions, as described by Gasparatos et al (2019). Two distinct medium sand layers (interbedded with a very fine sand unit) form the remaining length of the core. Comprised of quartz-mica sand, which is documented in various locations across the Murrumbidgee fan (Suresh et al., 2014), these poorly sorted swash zone sediments fine upwards and have erosive contacts with the finer sand bodies below them, which are difficult to identify due to the compression of the push tube drill. The lowest unit is a grey silt deposit, likely deflated from the original lakebed. The bulk of the upper phase B unit (figure 5.2.2) is characterised by 2 distinct sedimentary units. A very silty, medium sand, red in colour sits atop of the unit and is classed as a 'swash zone' deposit. This very poorly sorted unit diffusely transitions into a massive brown/ red silt unit (deflated) with a small amount of medium sand, distinctly rich in columnar calcretions. The upper phase B sediments provide evidence of deflated bed material undergoing successive pedogenesis, similar to the Golgol unit described by Bowler and Price (1998). Such a correlation, though speculative, would imply an approximate minimum age of 141 ± 35 ka (Fitzsimmons et al., 2014).

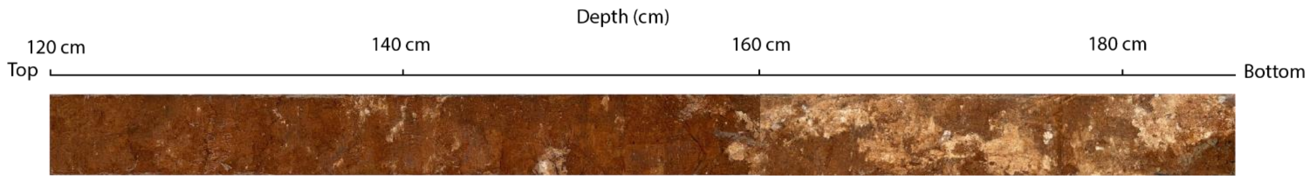

Figure 5.2.2 – Upper phase B sediments, taken from the SC10 core. This section of core shows a massive brown/red silt unit with distinct columnar calcite deposits in the lower length of the core. The upper section of this core, with its minor medium sand component is similar to the 'Golgol' unit first described by Bowler (1998). Under the assumption that the Golgol unit and Lake Sunrise Phase B sediments were deposited contemporaneously, they are likely >141 ± 35 ka in age (Fitzsimmons et al., 2014).

Phase C: > 90 ka

Sediments in the phase C unit are inferred to be > 90 ka, diffusely underlaying the deepest OSL samples taken from Phase D. This layer is comprised of massive sandy clay with a distinct yellow/ grey hue. Fe – Mn infilled rhizomorphs are prominent (figure 5.2.4), resulting from bioturbation on the dune surface (Gadd, 2007). Bioturbation has destroyed any fine silt laminations which may have been preserved in this dominantly silty layer. Light laminar calcareous banding appears in the lowest part of this unit (figure 5.2.5). It is likely that phase C represents a period of regular lakebed exposure, with oscillating periods of low lake levels, allowing for low laying vegetation to establish on the dune crest.

Figure 5.2.4 – Fe-Mg rhizomorph infill, part of the Phase C unit (bottom of SC8 core).

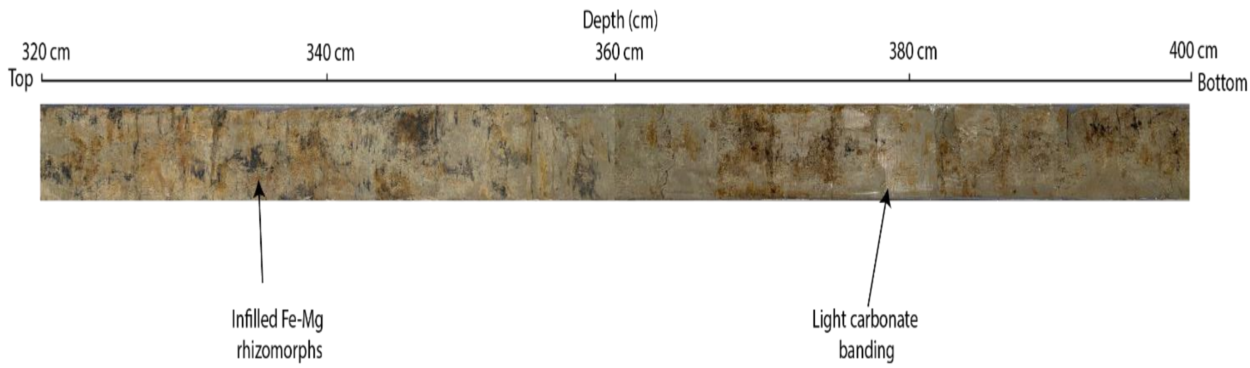

Figure 5.2.5 – Phase C sediments, taken from SC8 core. This section shows massive sandy clays with visible Fe-Mg rhizomorphic infill as well as light carbonate banding. The banding structure have been somewhat disturbed during the core opening process.

Phase D: 90 – 74 ka

The oldest sediments taken for OSL analysis come from the phase D unit. This unit extends from the inner base of the outer lunette (SC7) up to the crest of the lunette (SC9) (figure 5.2.1(b)). Erosive contact with the underlaying phase C silts suggests a rapid onset lake full conditions and the deposition of medium – coarse swash zone sediments (figure 5.2.6). The shoreface moderately slopes westward, with sediments fining away from the lake basin. This clean sand unit, dominantly quartz also increases in silt content away from the lake basin, indicating there were likely intermittent periods of lakebed deflation during this time of enhanced fluvial activity. The water table during this period would have oscillated between breaching the surface of the lake (filling it to a low level) and sitting just below the surface (exposing the lake bed). Any silt content at the base of the lunette was likely reworked further up the lunette structure, hence the low silt content at the base of the lunette (SC7, figure 5.2.1(b)).

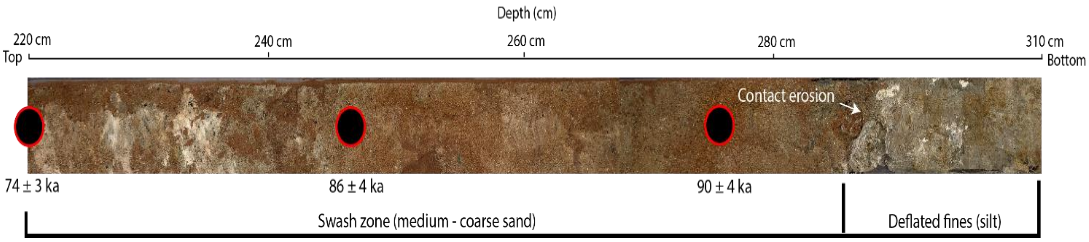

Figure 5.2.6 – Phase D sediments, taken from the SC7 core. This section of core shows the contact erosive boundary between the coarse phase D swash zone sediments, and the underlaying deflated silt material. Three OSL sample were taken for dating in the swash zone deposit, ranging from 90 – 74 ka.

Phase E – F: 74 – 69 ka

Phase E and F are a group of two distinct sedimentary units which were deposited rapidly (figure 5.2.7). The underlying group E sediments have a diffuse lower boundary to the swash zone sediments from phase D. The volume of coarse-medium grains from the phase D unit decreases to 0 % within 5 cm of the diffuse boundary, transitioning into a clean, red silt (100 % mud content) with blotchy carbonate inclusions. This sedimentological change reflects a shift in depositional regime, transitioning from consistently low lake levels to lakebed deflation and aeolian remobilisation of shoreline sediments. The receding water table, coupled with a reduction in local surface hydrological input has allowed for this assemblage of sediments to form. The transition to phase F is diffuse, and there is minimal colour change in the profile. Comprised of a silty sand that fines leeward (from coarse to fine), phase F is a remnant of the highest water levels experienced in the basin. The presence of coarse sand and silt together is likely resulting from the mixing (as a result of bioturbation, surface erosion and redeposition) of silts that were deflated following the period of prolonged lake full conditions, with sands previously deposited by waves and wind under lake-full conditions. This is the only phase in Lake Sunrise's history that overflow to the south-west may have been activated. It is very likely that groundwater discharge would have been very high with some surface discharge contributing to this filling event. The relatively high silt content in this upper phase is the result of deflation since the reduction in surface flow input and resulting contraction of the lake shoreline (approx. 69 ka) up until the present. Phase F, G and H are separated by perhaps the most notable geomorphic event in the lake basin; the contraction of the shoreline to the middle lunette structure, as seen in the figure at the end of this section (figure 5.2.1(b)).

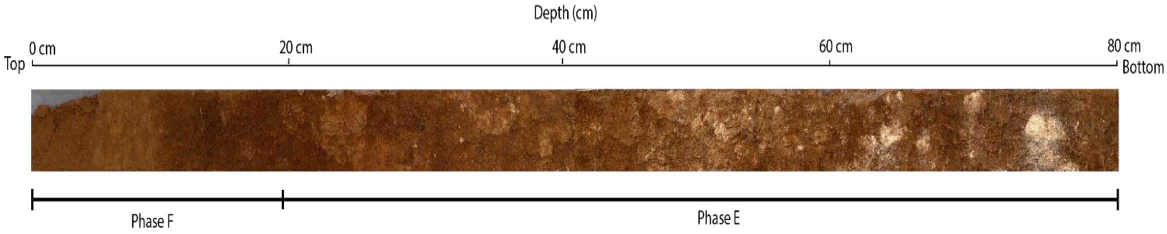

Figure 5.2.7 – Phase E - F sediments, taken from the SC8 core. This section of core shows the diffuse transition from deflated silty phase E sediments to the upper swash zone sediments from phase F.

Phase G: 74 - 69 ka

The phase G unit has been inferred in this study. It is likely comprised of deep lakebed material (typically muds) forming contemporaneously to the high lake levels of phase F. This unit was not physically observed through coring and sedimentological analysis, rather, inferred from its low topographic position in respect to the outer lunette.

Phase H: 69 – 45 ka

During phase H, the continuation of a consistent level of water residing in the lowest half of the basin, allowed for the middle lunette to form. It is likely that there are coarse swash zone sediments deposited deep below the extent of the SC5 core (located on the peak of the middle lunette crest), however this was not physically observed. The sediments atop of this inferred swash zone are very fine aeolian quartz sands, with minor medium sand and silt components. The lower half of this aeolian unit is chemically weathered, evident in the distinct change in colour from a rich red into a leached grey towards to bottom of the profile, indicating a period of dune stabilisation and soil formation sometime between 69 – 51 ka (figure 5.2.8). The lake oscillated between moderate and high-water levels, allowing for older swash zone sediments to be blown onto the crest of the middle dune.

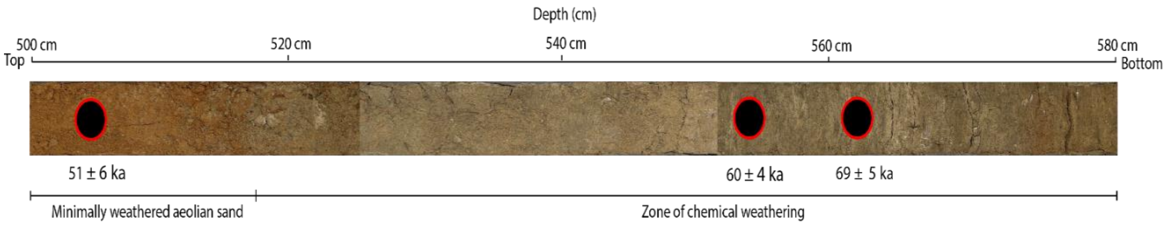

Figure 5.2.8 – Phase H sediments, taken from the SC5 core. This core is an aeolian deposit, comprised of a uniform very fine sand deposit throughout the entire length of the unit. Chemical weathering in the lower unit, seen in the transition between red and grey sediments, is evidence of dune stabilisation and pedogenesis sometime between 69 – 51 ka.

Phase I: 45 – 24 ka

During this phase, the first distinct beach deposits as part of the inner lunette complex begin accumulating on top of the older middle lunette. Episodic moderate and low lake levels allow for two distinct medium sand units to form, confided by intermittent fine sand (aeolian) units (figure 5.2.9). The medium-coarse grains in the lower beach deposit vary in colour, including black, red and white. The varied mineralogy of these grains in the lowest beach unit is indicative of an increasing amount of sediments sourced from local catchment discharge, resulting from enhanced surface water availability and catchment discharge. Grain size analysis of the SC4 sediments (average diameter 300 um) in comparison to the neighbouring Sunrise palaeochannel (average diameter 450 um) sediments reveal that although they are hydrologically disconnected from one another, these systems are responding contemporaneously to regional hydrological change. This is the most distinct indicator of surface flow being the dominant hydrological input to the lake basin rather than groundwater discharge. It is likely that towards the end of phase I, the water table may have risen in response to the increased aquifer recharge rates during a pluvial period, occurring contemporaneously with the upper most beach deposit during this phase, dated to 24 ka (see figure 5.2.9). This places an apparent hydrological 'lag' between surface and groundwater discharge of approximately 20'000 years.

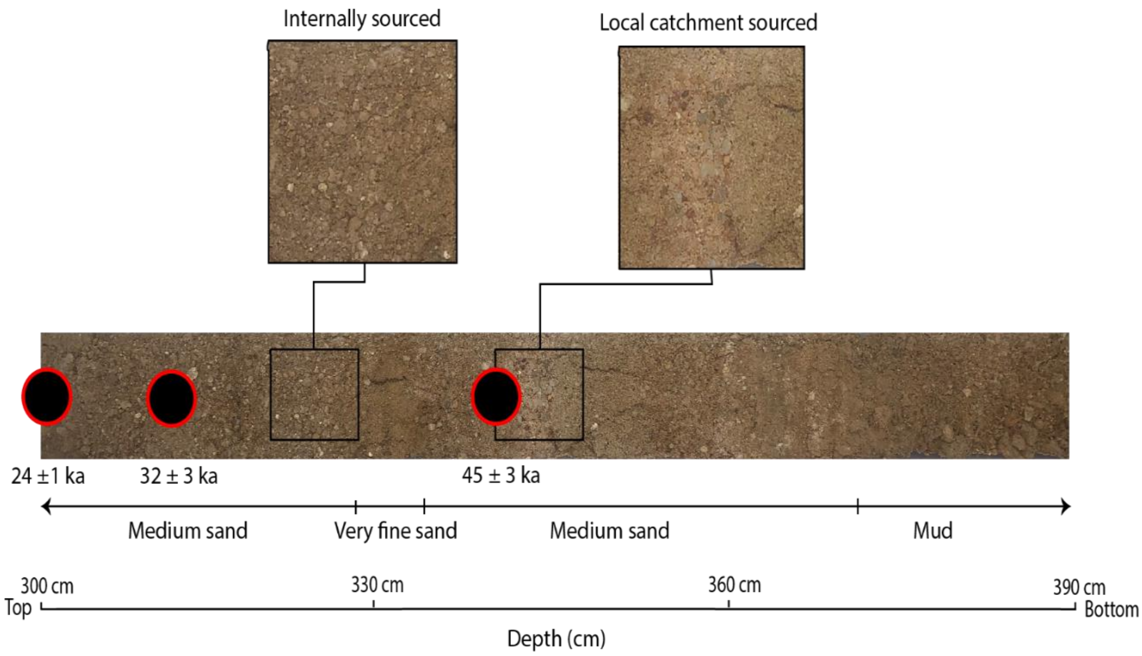

Figure 5.2.9 – Phase I sediments from SC4 core. This section shows the two beach deposits from the base of the inner lunette. The lower unit contains sediments locally sourced, evidenced by the variation in grain colour, whilst the upper unit contains white (clay stained) grains that are less influenced by local surface runoff. The OSL sample locations in the upper and lower beach deposits are presented as black and red dots. The median sediment size and depth are also indicated.

Phase J and present: < 24 ka

Phase J is final phase of major hydrological activity in the Lake Sunrise basin. A brown silty fine sand sits atop of two clean medium sand units, both of which fine leeward of the lake basin. The lower phase J unit is comprised of deflated fines with major calcite blotches. After the major hydrological activity seen in phase I, a short period of lake bed deflation occurred, followed by the onset of osscilating moderate to high lake levels. The upper swash zone of these two beach zones sits above the possible extent of a solely groundwater filled lake basin, so it can be inferred that the coupling of groundwater discharge and surface flow input to the Lake Sunrise basin post LGM was signifincant, allowing for water levels to reach the upper crest of the inner lunette. As per the OSL age depth modelling (figure 4.2.1), these two upper swash units likely occurred 11 – 9 ka and 7 – 2 ka respectively. Following this heightened hydrological activity, the aeolian remobilisation of beach sediments, as a response to the reduction in channel inflow andgroundwater discharge. In the modern day, these aeolian sediments have been slightly infilled with silt, resulting from a breif period of deflation. Stabilisation of lake bed and dune sediments is ongoing. Chemical weathering and pedogensis/ bioturbation are active processses on the dune surface. Groundwater discharge is nill, with the groundwater table sitting 26.8 - 32.5 m below the ground surface over a 50 year period (NSW Department of Primary Industries, 2021).

Table 5.2.1				
Phase	Age (ka)	Sedimentary description	Lake conditions	Palaeoenvironmental conditions
Modern	Modern	Light brown clayey sand with minor organic content (< 5 %). Sand likely sourced from bioturbated sandy units deeper in the lunette.	Hydrologically inactive. Groundwater discharge nil. Modern infill resulting from deflation and surface wash during rain events. Erosion of inner and middle lunettes following European settlement.	Recharge rates into the Murrumbidgee alluvium aquifer low, water depth at approximately 30 m below surface in local area (Water NSW, 2021). Average annual precipitation 500 mm/yr, average annual potential evaporation ~ 1800 mm/yr
J	< 24 ka	Light brown very fine dune sand with significant silt population (10-35 %). Silt population decreasing in volume away from lake basin. Two clean medium swash zone sand units, with minor very fine sand and deflation silt populations present, accompanied by a moderate amount of carbonate material.	Early short period of deflation during lakebed exposure followed by two distinct periods of intermittent lake full conditions (11 – 9 ka and 7 - 2 ka modelled) and aeolian remobilisation of beach sediments onto the dune crest. Groundwater discharge increasing up until the end of phase J.	Discharge into Lake Sunrise high sometime between 24 ka and present. A period of enhanced precipitation coupled with a high water table level would have allowed Lake Sunrise to be full.
I	45 – 24 ka	Inner lunette atop inner slope of middle lunette, Clean medium mixed swash zone sand units with intermittent fine dune sand units. Typically brown, however grains range in colour from white, red and black. Fine aeolian sediments deposited on top of middle lunette.	Episodic high and low lake levels characterised by distinct beach deposits which are then windblown as the water level recedes. Groundwater discharge initially low, but increasing drastically by the end of phase I.	The increase in pluvial activity leading to gradual recharge of Murrumbidgee alluvium aquifer and discharge into Lake Sunrise. OSL chronology showing 20'000 year lag between enhanced pluvial activity and total aquifer recharge. Activation of nearby Murrumbidgee palaeochannel (46 ka) evidence of regional surface hydrological activity.
H	69 – 45 ka	Upper phase H characterised by large deposit of very fine aeolian dune sand with minor medium swash zone sand and silt deflated component. Weathering in the lower half of the unit indicative of soil formation and dune stabilisation. Carbonates and Fe – Mg	Middle lunette activation. Cyclical moderate and low lake levels. Reduction in groundwater discharge allowing for accumulation of aeolian dune sand on crest of lunette for ~ 25'000 years.	Prolonged period of hydrological inactivity. Murrumbidgee alluvium aquifer experiencing low recharge rates resulting in a falling water table.

		infilled rhizomorphs present in sparse quantities throughout entire unit.		
G		Former deep lake bed	Oscillating low lake levels and exposed lakebed. Concentrated around the deepest, western section of the lake. Thin sheet of deflated bed material accumulating over outer lunette structure (phase F).	Groundwater discharge gradually reducing as recharge rates into the Murrumbidgee Alluvium aquifer decline.
F	74 – 69 ka	Red pedogenic silty sand, modal diameter fining (coarse sand to very fine sand) away from the lake basin.	Short lived period of lake full conditions in which the Lake Sunrise outflow channel would have been active. Cessation of phase F characterised by contraction of lake basin from the outer to middle lunette complex.	Local aquifer recharge high during brief period of enhanced pluvial conditions. Groundwater discharge breaching surface in lowest section of Lake Sunrise.
E		Dominantly red silty layer with some fine – medium sand inclusions crest ward, likely reworked phase D quartz sands.	Lakebed deflation and aeolian reactivation of dune sediments occurring contemporaneously. Water table well below surface.	Aquifer recharge 'lag' following pluvial phase D. The water table too low to discharge into Lake Sunrise.
D		Clean quartz sand unit at base of lunette, fining and increasing in silt content away from the lake basin.	Prolonged period of lake moderate – full conditions. Longest period of hydrological activity on the outer lunette.	Local increasing pluvial conditions. Groundwater discharge into Lake Sunrise is low, however recharge into the Murrumbidgee alluvium aquifer slowly increasing. Recharge into aquifer from local and regional pluvial activity.
C	90 – 74 ka	Grey/ brownish muddy unit, some medium sand inclusions basin ward. Extensive iron nodules and small traces of calcareous banding.	Contraction of lake basin. Period of stabilisation. Deeper sediments may reveal multiple compounding shorelines atop of each other.	Contraction of lake basin coinciding with absence of pluvial activity and oscillating low / moderate groundwater discharge lagging from the late phase B pluvial episode.
B		Divided into upper and lower phase. Upper: Red pedogenic silty sand unit overlaying silt unit, characterised by a brown/ red matrix with large calcareous inclusions. Diffuse transition to blotchy	Upper: Distinct, prolonged period of lake floor deflation with a reducing water table. Lake full conditions ensue a rising water table and increased pluvial activity. Lower: Episodic rising and falling lake levels with intermittent periods of dune	Upper: Prolonged absence of surface groundwater discharge, Murrumbidgee alluvium aquifer likely reducing in water volume. A final surge of pluvial activity allowing water levels to rise in the lake.

	~ 141 ka	grey and red sand (very fine) with consistent Fe - Mg inclusions. Lower: Diffuse transition into gold/ grey clean medium quartz-mica sand unit with a single very fine sand unit part way through this unit. Yellow silt unit at base of phase B.	stabilisation. Water table high, lake levels responding to external hydrological input.	Lower: Groundwater discharge controlling water levels in the lake basin, likely responding to the lagged input from an older pluvial episode. Regional recharge into Murrumbidgee alluvium aquifer reducing.
A		Unknown underlaying sedimentary system. Possibly ancient fluvial or lacustrine sediments of Shepparton formation. Similar to Lake Mungo (Douglas, 1996), or nearby Lake Gunbar (NSW Water, 1962).	Unknown	

5.3 – Hydrological balance of Lake Sunrise

Understanding the water balance model of a lake system is a powerful means of identifying changes to regional hydrology over vast temporal periods. It is vital for hydrological models to consider all pathways of discharge and water loss, which can be easily quantified through simple water balance equations (Nijssen et al., 2001, Schewe et al., 2014). Simple equations to calculate water balance in a lake, as adapted from Mason (et al., 1994) are as follows:

Water balance equation:

$$W_b = (Q_r + P + Q_G) - (E + Q_o + G_r) \quad \textit{(Equation 1)}$$

W_b = Annual water balance of lake (mm)

Q_r = Runoff discharge into lake (mm)

Q_G = Groundwater discharge into lake (mm)

P = Precipitation directly into lake (mm)

E = Evapotranspiration directly off lake (mm)

Q_o = Outflow discharge from lake (mm)

G_r = Groundwater recharge from lake (mm)

Whereby, the runoff **discharge into the lake (Q_r)** from runoff is calculated by:

$$Q_r = Q_c / A_L \; / 1000 \qquad \textit{(Equation 2)}$$

And

$$Q_c = (P_a \times (A_c - A_L) \times R_f \times 1000) \qquad \textit{(Equation 3)}$$

Q_c = Catchment discharge (m^3)

A_c =Catchment area (m^2)

A_L = Lake surface area (m^2)

R_f = Runoff factor

P_a = annual average precipitation (mm)

In this thesis, this equation is being utilised to understand the pathways by which the lake can be filled to the observed palaeoshorelines. Outflow discharge (Q_o) is zero (i.e. no overflow) at the level of the observed shorelines in the stratigraphic record. By assuming groundwater recharge (G_r) and groundwater discharge (Q_d) are zero, the efficacy of precipitation and runoff in the lake hydrology can be explored.

The variables of equations 1 – 3 were manipulated to try understand the role of *P* (precipitation, mm), *Aridity index* (AI) (P/PE, Trabucco and Zomer, 2009) and R_f (Runoff factor) in the possible filling of Lake Sunrise through surface discharge (Q_d) only (figure 6.3.1). Under the modern hydrological regime (~ 500 mm annual precipitation, BOM, 2021) and aridity index (0.25 AI), the water budget of Lake Sunrise is negative, consistent with landholder observations that the lake has not filled in the past 70 years as well as the observed cover of grey box (*Eucalyptus microcarpa*) on the lake floor. This calculated AI is consistent with the AI's experienced at other major lake sites in NSW (Mungo = 0.2 AI, George = 0.58 AI, Urana = 0.38 AI) (Trabucco and Zomer, 2009).

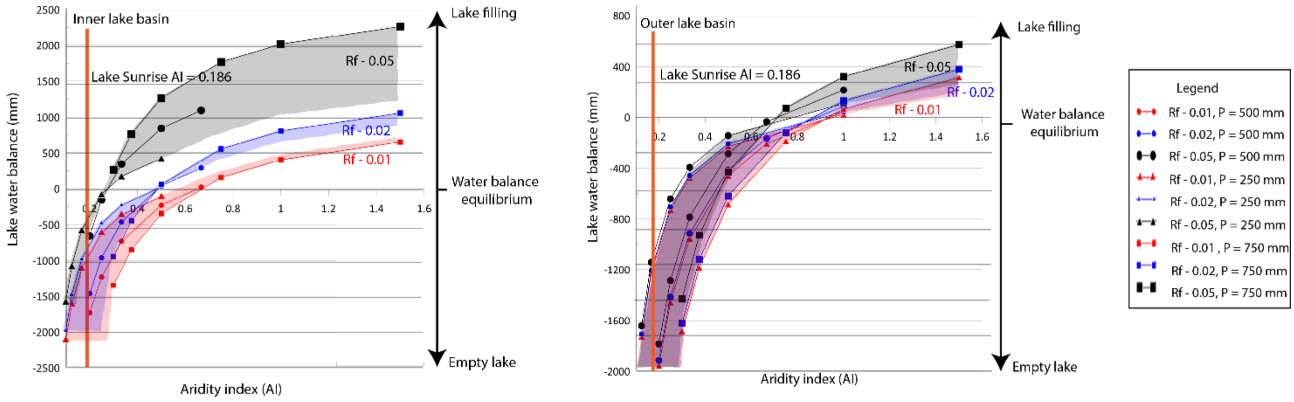

Figure 6.3.1 –Lake water balance response (mm) to aridity index (AI) under several precipitation and runoff factor variations for the inner (left) and outer (right) Lake Sunrise systems. Red indicates a runoff factor of 0.01, blue 0.02 and black 0.05. Data point shape represent different precipitation volume scenarios applied to the model (triangle = 250 mm/yr, circle = 500 mm/yr, square = 750 mm/yr) under which evaporation is varied to generate different AI values. The orange line indicates the modern aridity index at Lake Sunrise (AI = 0.186).

Figure 6.3.1 shows the response of lake water balance (mm) to aridity, under a range of runoff factors (Rf - 0.01, 0.02, 0.05), precipitation values (250 mm, 500 mm, 750 mm) and potential evaporation rate. Modelling of the outer lake basin (figure 5.3.1 - right) demonstrates the difficulty of filling the lake under any realistic climatic scenario. Equilibrium is attained between 0.7 - 0.9 AI and a maximum observed water balance from surface discharge occurs at 571.01 mm/yr, from which it would take ~ 15 years of persistent conditions to fill, ignoring the variability of dry and wet years affecting the water balance of the lake. Notably, this lake is relatively insensitive to variations in runoff factor or annual precipitation, but it is sensitive to the balance between P/PE, especially at lower levels. However, it could be speculated that a significant increase in catchment size may provide more substantial grounds for filling the lake through surface discharge. The inner lake (figure 5.3.1, left) is evidently more sensitive to changes in the modelled factors. The spread of hydrological equilibrium in response to the change in runoff factor is far greater in this smaller basin, ranging from 0.27 – 0.68 AI. Under the most enhanced precipitation model (750 mm, 0.05 runoff factor), lake balance tops out at 2265 mm/yr. Under conditions most similar to low elevation catchments today, with runoff factor around 0.01 (Hesse at al., 2018) the highest AI's would be required (under any of the modelled precipitation scenarios) to balance the water budget. These results indicate that a small lake size, coupled with a wetter hydrological regime and greater runoff efficiency lead to conditions conducive to lake budget equilibrium. The required conditions are suggestive of modern conditions in some of the most humid regions of south-eastern Australia, capable of maintaining permanent fresh water lakes. Specifically, AI up to 3 x more humid than that of today and/or runoff factor up to 5x that of today. Such substantial changes are considered unrealistic given the general consensus of drier (not wetter) climate in the most extreme phase of the last glacial cycle, although some increase of these factors is suggested by the presence of the large palaeochannels on the Riverine Plain (Hesse at al., 2018). It can be concluded that Lake Sunrise has been a dominantly groundwater supplied lake, especially when the lake was largest, although the accurate quantification of surface discharge contributing to major filling events throughout the Quaternary is not possible. To further test the hypothesis that groundwater discharge is central to the activation of this lake, particularly to the levels observed in the sedimentological record, Equation 4 uses the difference between the observed lake level (mm) derived from sedimentological analysis, and possible lake level (mm) from surface discharge alone to understand the volume of groundwater discharge (mm) required to fill the lake. Equation 1 is reorganised to calculate groundwater discharge (Q_G). The groundwater discharge equation applied to Lake Sunrise is as follows:

Groundwater discharge equation:

$$Q_G = O_L - (Q_d + P) - (E + Q_o + G_r) \text{ (Equation 4)}$$

O_L = Observed approximate lake level from sedimentological analysis (mm)

Table 5.3.1

Lake complex	***P*** (Annual precipitation, mm)	Aridity (AI)	***R_f*** (Runoff factor, %)	***Q_d*** *(Surface discharge into lake, mm)*	***Q_G*** *(Groundwater discharge, mm) required to fill lake*
Inner lake (1.15 km^2)	250	1.0	0.05	670.97	7329.03
	500	1.0	0.05	1343.14	6656.86
	750	1.5	0.05	2015.10	5984.9
Outer lake (7.2 km^2)	250	1.0	0.05	107.20	7892.8
	500	1.0	0.05	214.53	7785.47
	750	1.5	0.05	571.01	7428.99

* Catchment area derived from ArcMap hydrological modelling ~ 69 km^2

Water balance summary table 5.3.1 shows the results from modelling under the least arid (> 1.0), highest runoff factor (0.05 %) and varied precipitation (250 – 750 mm) conditions. All calculations can be found in appendix 8.1 With an observed lake level of 8000 mm in both the inner and outer lunette complexes, even under unrealistically wet climates, it is an impossibility to fill both the inner and outer Lake Sunrise basins purely with surface discharge.

5.4 – Groundwater response to Quaternary hydrological change in south-eastern Australia.

In this section, using Lake Sunrise as an independent hydrological archive, the response of local groundwater discharge is compared against other Quaternary environmental proxies in the region to uncover the relationship between surface and aquifer hydrology (Figure 5.4.1).

5.4.1 MIS 5 (~ 130 – 71 ka)

Marine oxygen isotope (MIS) stage 5 is characterised by enhanced hydrological activity throughout south-eastern Australia, much greater than that of today. Effective precipitation during this phase was higher than the modern day, driving speleothem growth in Naracoorte Caves, South Australia (Ayliffe et al., 1998). The availability of water through vegetation, which can be used as an analogue of atmospheric temperature during summer, is evidenced by $\delta^{18}O$ extracted from Dromaius (emu) eggshells, dating back to 87 ka in the Murray Darling basin (Miller et al, 2017). Australia's arid interior lakes were extremely high, with Lake Mega-Frome filled ~ 70 times its modern water volume and Lake Mega-Eyre similarly full (Nanson et al., 1998). The palaeochannels of the modern Murrumbidgee River, specifically the 'Coleambally phase' as coined by Page (et al., 1996) which reveal a period of enhanced fluvial discharge between ~ 110 – 80 ka. Hesse (et al., 2018) quantified the discharge and size of the Coleambally palaeochannel system, showing it was1.9 – 2.5 times wider and had a bankful discharge 4 – 8 times greater than that of today. Discussed is the attribution to temperature as the primary mechanism behind these enhanced channels, particularly as it influences the means by which available surface water is stored, vegetation (influencing runoff rates) and increasing the potential for orographic rainfall. The activation of the outer Lake Sunrise basin 90 – 74 ka is likely a lagged response to the enhanced surface discharge experienced in the region throughout MIS5 (Figure 6.4.1) of up to ~ 15,000 – 20,000 years. Scanlon (et al., 2006) show that recharge rates over large regions (40 – 300,000 km ^{2}) are often between 0.01 – 5 % of annual precipitation. At the given 0.1% recharge rate, given the current water table depth of 30 m, and average annual precipitation in the Murray Darling basin ~ 500 mm/yr, it would take up to 16,000 years to approach aquifer water volumes high enough for groundwater to reach the levels seen in the Lake Sunrise basin in MIS5.

5.4.2 MIS 4 (~ 71 – 57 ka)

There is conflicting evidence of both enhanced and reduced surface hydrological activity throughout MIS4. A distinct period of enhanced aeolian activity in the Mallee dune fields in the western Murray Basin from 72-63 ka (Lomax et al., 2011) and absence of major paleochannels activity in the Murray-Darling Basin suggest that there was a period of reduced hydrological activity during MIS4 (Page et al., 1996). Speleothem records also validate this observation, as there was an apparent absence of available moisture throughout this period (Ayliffe et al., 1998). Lake Mungo, 200 km to the west of Lake Sunrise, was also hydrologically inactive, as detailed by Jankowski et al. (2020) and Fitzsimmons et al. (2014). Contradicting this are the heightened water levels seen at Lake Frome and Lake Callabonna (Cohen et al., 2011), although these may have been fed by rivers draining the northern part of the Lake Eyre Basin (Nanson et al., 2008). This enhanced surface water availability is again confirmed by $\delta^{18}O$ extracted from *Dromaius* eggshells along the lower Darling River (Miller et al, 2017). As seen in figure 6.4.1, groundwater discharge at Lake Sunrise throughout this period gradually reduced, as seen in the increasing volume of aeolian dune sand terminated by the onset of lake-bed deflation. Activity on the Gulgo palaeochannel of the Lachlan River (including Lake Mungo) (Kemp and Rhodes, 2010) suggest that increase in discharge from the Murrumbidgee alluvium aquifer continued to persist during a time of enhanced surface water activity. The persistence of a lake and groundwater discharge in Lake Sunrise suggests that: a) that groundwater recharge experienced during MIS5 was substantial enough to retain a high-water table and was amplified during a wet MIS4, and b) during MIS4 the groundwater recharge rate began to decline as the fluvial conditions during MIS4, although still greater than today, were insufficient to achieve an equilibrium or surplus of groundwater recharge compared to the MIS5 wet conditions.

5.4.3 MIS 3 (57 – 29 ka)

The consensus is that conditions were generally more humid across the Australian continent during early MIS3. Enhanced moisture availability in speleothems (Ayliffe et al., 1998) and increased $\delta^{18}O$ extracted from *Dromaius* eggshells suggest that between 55 – 45 ka (Miller and Fogel, 2016), precipitation was still persistently enhanced when compared to today, similar to the conditions experienced during MIS5. During this time Lake Mungo was perennial and experienced lake full conditions for a sustained 15,000-year period (Jankowski et al., 2020), coinciding with the 'Kerarbury phase' of the Murrumbidgee palaeochannel network, whereby bankfull discharge was ~ 260 x greater than that of the modern Murrumbidgee (Hesse et al., 2018). Both are evidence of heightened fluvial activity, resulting from increased discharge in both the Lachlan and Murrumbidgee headwater catchments in the Australian highlands. Both coincide with the increased water levels at Lake George, testament to the higher availability of moisture in Australia's southern highlands (Jankowski et al., 2021). The fluvial activity seen in the Murrumbidgee palaeochannel near Lake Sunrise at ~ 46 ka further attests to the notion of enhanced fluvial discharge during this period. Lake levels at Lake Sunrise reached their lowest point, drying completely, between 45-50 ka before increasing by 45 ka, whereby the inner lake basin was activated. Another brief interval of lower lake levels was followed by another highstand from at least 32 ka to 24 ka. The high lake levels towards the end of MIS3 imply a delayed response (~ 15,000 years) to surface water availability earlier in MIS3. The increasing aridity in the Murray-Darling Basin ~ 30 ka (late MIS3), (Miller et al, 2017) resulted in declining water levels at Lake George (Jankowski et al., 2021), yet enhanced maximum bank full discharge in both Murrumbidgee and Lachlan palaeochannel systems, as well as heightened water levels at Lake Mungo were prevalent (Bowler et al., 2003, Jankowski et al., 2020, Fitzsimmons et al., 2014).

It is likely that during this time, increased annual snowmelt from the highlands (Reinfelds et al., 2014; Barrows et al., 2002) would have led to the creation of these great channels (Hesse et al., 2018), even though effective precipitation rates would have been lower approaching the LGM.

5.4.4 MIS 2 (29 – 12 ka)

The peak of the LGM occurred at ~ 24.5 ka (Barrows et al. 2002). Conditions were cooler and drier than that of today, resulting in an increased dust flux in the southern Australia region (Hesse, 2004). The palaeochannels of the Riverine plain were operating at their greatest bankfull capacity during this time (Hesse et al., 2018), It is likely that during this time, increased annual snowmelt from the highlands (Reinfelds et al., 2014; Barrows et al., 2002) would have led to the creation of these great channels (Hesse et al., 2018), even though precipitation rates would have been lower approaching the LGM. Lake levels at Mungo, during what is coined the 'Arumpo phase', may have oscillated from dry to deep (Fitzsimmons et al., 2014), responding to this seasonal discharge from the Lachlan River catchment (Hesse et al., 2018), with 'mega-lake' conditions observed at ~ 26 – 22 ka (Bowler et al., 2003, Fitzsimmons et al., 2014, Jankowski et al., 2020). Increased aridity, as derived from decreased $\delta^{18}O$ % from *Dromaius* eggshells (Miller et al, 2017), further supports the idea of a cool, dry LGM. The increase in dust flux from the south-eastern Australian interior during the LGM, identified in Tasman Sea sediments, further confirms the presence of arid conditions (Hesse, 1994). The apparent absence of foreshore building at the Luckdale site at Lake George during the peak of the LGM also coincides with these drier conditions. However, Jankowski et al. (2020) noted previous reporting of construction of a beach facies at the northern end of the lake and suggest that the absence of an equivalent unit at Luckdale may be due to continual reworking of the material. Alternatively, Jankowski et al. (2020) suggested that the northern beach may be affected by errors in the multi-aliquot thermoluminescence dating technique (Fullagar et al., 1996).During the peak of the LGM, Lake Sunrise experienced oscillating lake levels, that were moderate – high in late MIS3/ early MIS2, slowly increasing until the inner lake basin was full at some point just before the LGM. This increasing groundwater discharge is likely related to recharge lag from the onset of enhanced fluvial conditions experienced during early MIS3 some 20,000 years earlier. Coupled with the low evaporation rates, a function of average temperatures 8-9 °C cooler than today (Miller et al., 1997), there would have been a positive water balance in Lake Sunrise.

5.4.5 MIS 1 (12 ka – present)

The Holocene was a period of rapid environmental change in response to the cessation of the LGM. During this time, there was a noticeable reduction in fluvial activity across the entire MDB. The 'Yanco' system gave way to the modern Murrumbidgee system, substantially smaller than the immensely wide LGM Yanco palaeochannel (Hesse et al., 2018). The desiccation of Lake Mungo, in response to the avulsion of Willandra Creek (Kemp et al., 2017), to the modern (and smaller) Lachlan River may or may not be related to the declining seasonal bankful discharge events seen throughout the MDB in the Holocene (Hesse et al., 2018; Ogden et al., 2001). Aridity was decreasing throughout this time (Miller et al., 2017), however the effective precipitation was unable to generate sufficient surface runoff to establish palaeochannels similar to those seen in MIS2, 3 and 5 most likely because of the increased vegetation cover and decreased winter snowpack (Hesse et al., 2018). The transition to smaller, meandering channels throughout the Holocene climatic optimum (Fitzsimmons et al., 2013) have persisted into the more arid late stage of the Holocene. A final (undated) shoreline from the Lake Sunrise inner basin suggests that there were high lake levels at some point between the LGM and the present. Based on the groundwater discharge lag experienced during other MIS phases, it could be speculated that the last lake full event at Lake Sunrise occurred ~ 15,000 – 20,000 years after the peak of the LGM, placing it around 5 ka. Since then, the water table has fallen well below the surface, and Lake Sunrise has been largely inactive. The presence of black-box gums (*Eucalyptus largiflorens*) in the lake bed is evidence of modern hydrological inactivity, as these trees typically thrive in dry, nutrient rich soils that are rarely inundated (Rawlings et al., 2010).

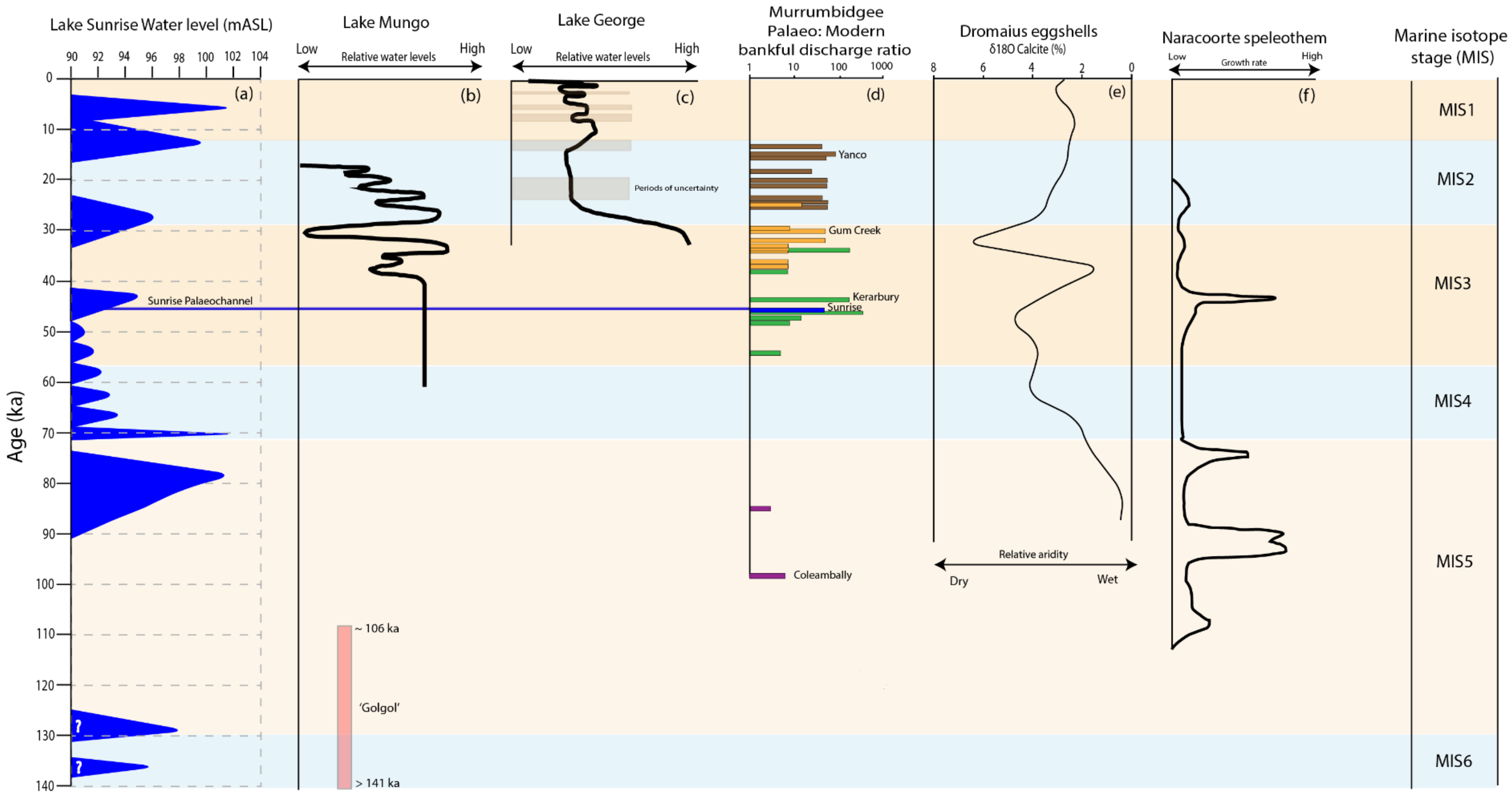

Figure 6.4.1 – Comparative figure showing various environmental proxies from Australia. (a) Reconstructed lake levels for Lake Sunrise, showing the response of a groundwater system as well as nearby palaeochannel. (b) The relative water level from Lake Mungo, NSW has been adapted from Fitzsimmons (et al., 2014). (c) The relative water level at Lake George has been reconstructed from Jankowski (et al., 2021), highlighting the zones of reconstruction uncertainty. (d) Palaeo:Modern bankful discharge of Murrumbidgee palaeochannels (Hesse et al., 2018). (e) Relative aridity, calculated from $\delta^{18}O$ calcite (%) extracted from *Dromaius* eggshells throughout central Australia (Miller et al., 2017). (f) Naracoorte speleothem growth rate (Ayliffe et al., 1998).

6 Conclusions and recommendations

6.1 Conclusions

The aims of this study were successfully addressed:

- The study successfully reconstructed the Quaternary evolution of the Sunrise Basin using a chronostratigraphic and sedimentological framework. OSL age estimation places the Lake Sunrise basin as early as ~ 90 ka (MIS 5). The chronostratigraphy from the lake basin suggests a unique history of lakebed desiccation and groundwater discharge in the low laying zones of the riverine plains and suggests a new avenue of research into the detailed groundwater hydrological response to environmental change throughout the Quaternary in Australia.
- The successful hydrological modelling of Lake Sunrise demonstrated the inability of surface discharge to fill the lake, rather, it relies on groundwater discharge to fill. This is starkly different to surrounding lakes that have been studies, particularly Lake Mungo, highlighting the need to consider new pathways for hydrological input to Lake systems on the Riverine plains. Thus, Lake Sunrise is the perfect independent hydrological proxy for groundwater evolution throughout the Quaternary.
- Analysis of Lake Sunrise to other Quaternary proxies reveals that it lags hydrologically behind fluvial and lacustrine systems in the same region. Novel water balance modelling suggests that an approximate of 10,000 – 20,000 years between regional surface recharge following an enhanced hydrological period and the subsequent discharge of groundwater into Lake Sunrise was observed.

6.2 Recommendations

There are several field, laboratory and writing changes that would increase the potency of this study for future publications. An increased number of 'groundwater discharge lakes' would be incredibly useful as a means of comparison for this study, as it would test the validity of the sedimentological assumptions made throughout this thesis. Further OSL dating, particularly of the upper sediments, is required to refine the lake level history of Lake Sunrise and the hydrological lag between regional groundwater recharge and groundwater discharge into Lake Sunrise. By doing this, the age vs depth modelling would be more easily refined and produce more representative projections. Further laboratory analysis of the water retention capabilities of differing grain sizes would also be incredibly meaningful for estimating long term water content, as this seems to play an important role in the attenuation of environmental dose in the analysed samples.

7. References

Aitken, M.J., 1998. Introduction to optical dating: the dating of Quaternary sediments by the use of photon-stimulated luminescence. Clarendon Press.

Atterberg, A.,1911. Uber die physikalische Bodenuntersuchung und u¨ ber die Plastizita¨t der Tone. Internationale Mitteilungen fu¨ r Bodenkunde, 1, 10–43.

Australian Bureau of Meteorology. 2021. Climate, Wind speed and direction rose - Hay. [online] Available at: <http://www.bom.gov.au/cgibin/climate/cgi_bin_scripts/windrose_selector.cgi?period=Annual&type=9&location=75031&Submit=Get+Rose> [Accessed 2 August 2021].

Ayliffe, L.K., Marianelli, P.C., Moriarty, K.C., Wells, R.T., McCulloch, M.T., Mortimer, G.E. and Hellstrom, J.C., 1998. 500 ka precipitation record from southeastern Australia: evidence for interglacial relative aridity. Geology, 26(2), pp.147-150.

Barrows, T.T., Stone, J.O., Fifield, L.K. and Cresswell, R.G., 2002. The timing of the last glacial maximum in Australia. Quaternary Science Reviews, 21(1-3), pp.159-173.

Barrows, T.T., Fitzsimmons, K.E., Mills, S.C., Tumney, J., Pappin, D. and Stern, N., 2020. Late Pleistocene lake level history of Lake Mungo, Australia. Quaternary Science Reviews, 238, p.106338.

Bateman, M.D., Frederick, C.D., Jaiswal, M.K. and Singhvi, A.K., 2003. Investigations into the potential effects of pedoturbation on luminescence dating. Quaternary Science Reviews, 22(10-13), pp.1169-1176.

Bateman, M.D., Boulter, C.H., Carr, A.S., Frederick, C.D., Peter, D. and Wilder, M., 2007. Detecting post-depositional sediment disturbance in sandy deposits using optical luminescence. Quaternary geochronology, 2(1-4), pp.57-64.

Bell, W.T. and Zimmerman, D.W., 1978. The effect of HF acid etching on the morphology of quartz inclusions for thermoluminescence dating. Archaeometry, 20(1), pp.63-65.

BOM. 2021. Annual climate statement 2020. [online] Available at: <http://www.bom.gov.au/climate/current/annual/aus/> [Accessed 29 September 2021].

Bøtter-Jensen, L. and Mejdahl, V., 1988. Assessment of beta dose-rate using a GM multicounter system. International Journal of Radiation Applications and Instrumentation. Part D. Nuclear Tracks and Radiation Measurements, 14(1-2), pp.187-191.

Bowler, J.M., Jones, R., Allen, H. and Thorne, A.G., 1970. Pleistocene human remains from Australia: a living site and human cremation from Lake Mungo, western New South Wales. World archaeology, 2(1), pp.39-60.

Bowler, J.M., 1976. Aridity in Australia: age, origins and expression in aeolian landforms and sediments. Earth-science reviews, 12(2-3), pp.279-310.

Bowler, J.M., 1978. Quaternary climate and tectonics in the evolution of the Riverine Plain, southeastern Australia. Landform evolution in Australasia, pp.70-112.

Bowler, J.M. and Teller, J.T., 1986. Quaternary evaporites and hydrological changes, Lake Tyrrell, north-west Victoria. Australian Journal of Earth Sciences, 33(1), pp.43-63.

Bowler, J.M. and Price, D.M., 1998. Luminescence dates and stratigraphic analyses at Lake Mungo: review and new perspectives. Archaeology in Oceania, 33(3), pp.156-168.

Bowler, J.M., Johnston, H., Olley, J.M., Prescott, J.R., Roberts, R.G., Shawcross, W. and Spooner, N.A., 2003. New ages for human occupation and climatic change at Lake Mungo, Australia. Nature, 421(6925), pp.837-840.

Bowler, J.M., Gillespie, R., Johnston, H. and Sporcic, K., 2012. Wind v water: glacial maximum records from the Willandra Lakes. In Peopled landscapes:(terra australis 34) archaeological and biogeographic approaches to landscapes. ANU ePress.

Brennan, B.J., 2003. Beta doses to spherical grains. Radiation Measurements, 37(4-5), pp.299-303.

Breitner, D., Arvela, H., Hellmuth, K.H. and Renvall, T., 2010. Effect of moisture content on emanation at different grain size fractions–A pilot study on granitic esker sand sample. Journal of environmental radioactivity, 101(11), pp.1002-1006.

Brook, G.A., Marais, E., Srivastava, P. and Jordan, T., 2007. Timing of lake-level changes in Etosha Pan, Namibia, since the middle Holocene from OSL ages of relict shorelines in the Okondeka region. Quaternary International, 175(1), pp.29-40.

Brown, C.M. and Stephenson, A.E., 1991. Geology of the Murray Basin, southeastern Australia. Bulletin-Australia, Bureau of Mineral Resources, Geology and Geophysics, (235).

Cohen, T.J., Nanson, G.C., Jansen, J.D., Jones, B.G., Jacobs, Z., Treble, P., Price, D.M., May, J.H., Smith, A.M., Ayliffe, L.K. and Hellstrom, J.C., 2011. Continental aridification and the vanishing of Australia's megalakes. Geology, 39(2), pp.167-170.

Cunningham, A.C., DeVries, D.J. and Schaart, D.R., 2012. Experimental and computational simulation of beta-dose heterogeneity in sediment. Radiation measurements, 47(11-12), pp.1060-1067.

Cunningham, A.C., Wallinga, J., Hobo, N., Versendaal, A.J., Makaske, B. and Middelkoop, H., 2014. Does deposition depth control the OSL bleaching of fluvial sediment?. Earth Surface Dynamics Discussions, 2(2), pp.575-603.

Datasets.seed.nsw.gov.au. 2021. NSW Hydrography. [online] Available at: <https://datasets.seed.nsw.gov.au/dataset/nsw-hydrography> [Accessed 10 August 2021].

Doeglas, D.J., 1968. Grain-size indices, classification and environment. Sedimentology, 10, 83–100.

Douglas, K., 1996. Land systems and stratigraphy of Lake Mulurulu: examination of Quaternary palaeoenvironments. Unpublished Honours Thesis, School of Earth Sciences, University of Melbourne.

Duller, G.A., 2008. Single-grain optical dating of Quaternary sediments: why aliquot size matters in luminescence dating. Boreas, 37(4), pp.589-612.

Elevation.fsdf.org.au. 2021. Elvis - Elevation and Depth - Foundation Spatial Data. [online] Available at: <https://elevation.fsdf.org.au/> [Accessed 4 August 2021].

Emiliani, C., 1966. Paleotemperature analysis of Caribbean cores P6304-8 and P6304-9 and a generalized temperature curve for the past 425,000 years. The Journal of Geology, 74(2), pp.109-124.

Farebrother, W., Hesse, P.P., Chang, H.C. and Jones, C., 2017. Dry lake beds as sources of dust in Australia during the Late Quaternary: A volumetric approach based on lake bed and deflated dune volumes. Quaternary Science Reviews, 161, pp.81-98.

Feathers, J.K. and Migliorini, E., 2001. Luminescence dating at Katanda—a reassessment. Quaternary Science Reviews, 20(5-9), pp.961-978

Field, J.P. and Pelletier, J.D., 2018. Controls on the aerodynamic roughness length and the grain-size dependence of aeolian sediment transport. Earth Surface Processes and Landforms, 43(12), pp.2616-2626.

Fitzsimmons, K.E., Bowler, J.M., Rhodes, E.J. and Magee, J.M., 2007. Relationships between desert dunes during the late Quaternary in the Lake Frome region, Strzelecki Desert, Australia. Journal of Quaternary Science: Published for the Quaternary Research Association, 22(5), pp.549-558.

Fitzsimmons, K.E., Cohen, T.J., Hesse, P.P., Jansen, J., Nanson, G.C., May, J.H., Barrows, T.T., Haberlah, D., Hilgers, A., Kelly, T. and Larsen, J., 2013. Late Quaternary palaeoenvironmental change in the Australian drylands. Quaternary Science Reviews, 74, pp.78-96.

Fitzsimmons, K.E., Stern, N. and Murray-Wallace, C.V., 2014. Depositional history and archaeology of the central Lake Mungo lunette, Willandra Lakes, southeast Australia. Journal of Archaeological Science, 41, pp.349-364.

Flemming, B.W., 2000, March. The role of grain size, water depth and flow velocity as scaling factors controlling the size of subaqueous dunes. In Marine sandwave dynamics, international workshop (pp. 23-24).

Folk, R.L., 1954. The distinction between grain size and mineral composition in sedimentary-rock nomenclature. The Journal of Geology, 62(4), pp.344-359.

Fontes, J.C., Coque, R., Dever, L., Filly, A. and Mamou, A., 1983. Paléohydrologie isotopique de l'oued el Akarit (Sud Tunisie) au Pléistocène supérieur et à l'Holocène. Palaeogeography, Palaeoclimatology, Palaeoecology, 43(1-2), pp.41-62.

Friedman, G.M., Sanders, J.E. and Kopaska-Merkel, D.C. 1992 Principles of Sedimentary

Fuchs, M. and Lomax, J., 2019. Stone pavements in arid environments: reasons for De overdispersion and grain-size dependent OSL ages. Quaternary Geochronology, 49, pp.191-198.

Fullagar RLK, Price DM, Head LM. 1996. Early human occupation of northern Australia: archaeology and thermoluminescence dating of Jinmium rock-shelter, Northern Territory. Antiquity 70: 751–773.

Ga.gov.au. 2021. Continental Geology Section | Geoscience Australia. [online] Available at: <https://www.ga.gov.au/about/projects/resources/continental-geology> [Accessed 4 August 2021].

Gadd, G.M., 2007. Geomycology: biogeochemical transformations of rocks, minerals, metals and radionuclides by fungi, bioweathering and bioremediation. Mycological research, 111(1), pp.3-49.

Galbraith, R.F. and Green, P.F., 1990. Estimating the component ages in a finite mixture. International Journal of Radiation Applications and Instrumentation. Part D. Nuclear Tracks and Radiation Measurements, 17(3), pp.197-206.

Galbraith, R.F., Roberts, R.G., Laslett, G.M., Yoshida, H. and Olley, J.M., 1999. Optical dating of single and multiple grains of quartz from Jinmium rock shelter, northern Australia: Part I, experimental design and statistical models. Archaeometry, 41(2), pp.339-364.

Gasparatos, D., Massas, I. and Godelitsas, A., 2019. Fe-Mn concretions and nodules formation in redoximorphic soils and their role on soil phosphorus dynamics: Current knowledge and gaps. Catena, 182, p.104106.

Guérin, G. and Mercier, N., 2011. Determining gamma dose rates by field gamma spectroscopy in sedimentary media: results of Monte Carlo simulations. Radiation Measurements, 46(2), pp.190-195.

Gunn, P., 2003. Interpretation of Gravity and Magnetic Data over the Oaklands Basin, New South Wales. NSW Department of Primary Industries, Report GS2003/308.

Hesse, P.P., 1994. The record of continental dust from Australia in Tasman Sea sediments. Quaternary Science Reviews, 13(3), pp.257-272.

Hesse, P.P., Williams, R., Ralph, T.J., Fryirs, K.A., Larkin, Z.T., Westaway, K.E. and Farebrother, W., 2018. Palaeohydrology of lowland rivers in the Murray-Darling Basin, Australia. Quaternary Science Reviews, 200, pp.85-105.

Huffman, G.G. and Price, W.A., 1949. Clay dune formation near Corpus Christi, Texas. Journal of Sedimentary Research, 19(3), pp.118-127.

Jackson, R.S., 2008. Wine science: principles and applications. Academic press.

Jacobs, Z., Duller, G.A., Wintle, A.G. and Henshilwood, C.S., 2006. Extending the chronology of deposits at Blombos Cave, South Africa, back to 140 ka using optical dating of single and multiple grains of quartz. Journal of Human Evolution, 51(3), pp.255-273.

Jacobs, Z., Wintle, A.G., Roberts, R.G. and Duller, G.A., 2008. Equivalent dose distributions from single grains of quartz at Sibudu, South Africa: context, causes and consequences for optical dating of archaeological deposits. Journal of Archaeological Science, 35(7), pp.1808-1820.

Jankowski, N.R., Stern, N., Lachlan, T.J. and Jacobs, Z., 2020. A high-resolution late Quaternary depositional history and chronology for the southern portion of the Lake Mungo lunette, semi-arid Australia. Quaternary Science Reviews, 233, p.106224.

Jankowski, N.R., Cohen, T.J., Larsen, J., Larsen, A. and May, J.H., 2021. Revisiting the abandoned shorelines of Lake George, Australia: a refined optical dating framework. Journal of Quaternary Science.

Junding, W.W.X., 1991. The measurement of annual dose from Th series and U series decay chains by thick source alpha counting [J]. Nuclear Techniques, 2.

Kemp, J. and Rhodes, E.J., 2010. Episodic fluvial activity of inland rivers in southeastern Australia: Palaeochannel systems and terraces of the Lachlan River. Quaternary Science Reviews, 29(5-6), pp.732-752.

Kemp, J., Pietsch, T., Gontz, A. and Olley, J., 2017. Lacustrine-fluvial interactions in Australia's Riverine Plains. Quaternary Science Reviews, 166, pp.352-362.

Lomax, J., Hilgers, A., Twidale, C.R., Bourne, J.A. and Radtke, U., 2007. Treatment of broad palaeodose distributions in OSL dating of dune sands from the western Murray Basin, South Australia. Quaternary Geochronology, 2(1-4), pp.51-56.

Lomax, J., Hilgers, A. and Radtke, U., 2011. Palaeoenvironmental change recorded in the palaeodunefields of the western Murray Basin, South Australia–new data from single grain OSL-dating. Quaternary Science Reviews, 30(5-6), pp.723-736.

Magee, J.W., 1991. Late Quaternary lacustrine, groundwater, aeolian and pedogenic gypsum in the Prungle Lakes, southeastern Australia. Palaeogeography, Palaeoclimatology, Palaeoecology, 84(1-4), pp.3-42.

Mason, I.M., Guzkowska, M.A.J., Rapley, C.G. and Street-Perrott, F.A., 1994. The response of lake levels and areas to climatic change. Climatic change, 27(2), pp.161-197.

Melton, F.A., 1940. A tentative classification of sand dunes its application to dune history in the southern High Plains. The Journal of Geology, 48(2), pp.113-174.

Miller, G.H., Magee, J.W. and Jull, A.J.T., 1997. Low-latitude glacial cooling in the Southern Hemisphere from amino-acid racemization in emu eggshells. Nature, 385(6613), pp.241-244.

Mueller, D., Jacobs, Z., Cohen, T.J., Price, D.M., Reinfelds, I.V. and Shulmeister, J., 2018. Revisiting an arid LGM using fluvial archives: a luminescence chronology for palaeochannels of the Murrumbidgee River, south-eastern Australia. Journal of Quaternary Science, 33(7), pp.777-793.

Nanson, G.C. and Price, D.M., 1998. Quaternary change in the Lake Eyre basin of Australia: an introduction. Palaeogeography, Palaeoclimatology, Palaeoecology, 144(3-4), pp.235-237.

Nanson, G.C., Price, D.M., Jones, B.G., Maroulis, J.C., Coleman, M., Bowman, H., Cohen, T.J., Pietsch, T.J. and Larsen, J.R., 2008. Alluvial evidence for major climate and flow regime changes during the middle and late Quaternary in eastern central Australia. Geomorphology, 101(1-2), pp.109-129.

Nielsen, P. and Hanslow, D.J., 1991. Wave runup distributions on natural beaches. Journal of Coastal Research, pp.1139-1152.

Nijssen, B., O'Donnell, G.M., Lettenmaier, D.P., Lohmann, D. and Wood, E.F., 2001. Predicting the discharge of global rivers. Journal of Climate, 14(15), pp.3307-3323.

NSW State Government 2018, Lachlan Alluvium Water Resource Plan, Department of Primary Industries, viewed 4th August 2018, https://www.industry.nsw.gov.au/__data/assets/pdf_file/0010/175969/Lachlan-alluvium-appendice-a-water-resource-description.pdf.

Ogen, R., Spooner, N., Reid, M., Head, J., 2001. Sediment dates with implications forthe age of the conversion from palaeochannel to modern fluvial activity on theMurray river and tributaries. Quaternary International 83–85, 195–209.

Orth, A., 1875. Bezeichnung des Sandes nach der Gro¨sse des Kornes. Neues Jahrbuch fu¨ r Mineralogie, 1875, 551.

Page, K., Dare-Edwards, A., Nanson, G. and Price, D., 1994. Late quaternary evolution of lake urana, new south wales, Australia. Journal of Quaternary Science, 9(1), pp.47-57.

Page, K., Nanson, G. and Price, D., 1996. Chronology of Murrumbidgee river palaeochannels on the Riverine Plain, southeastern Australia. Journal of Quaternary Science: Published for the Quaternary Research Association, 11(4), pp.311-326.

Picard, M.D., 1971. Classification of fine-grained sedimentary rocks. Journal of Sedimentary Research, 41(1), pp.179-195.

Prescott, J.R. and Hutton, J.T., 1994. Cosmic ray contributions to dose rates for luminescence and ESR dating: large depths and long-term time variations. Radiation measurements, 23(2-3), pp.497-500.

Price, W.A., 1963. Physicochemical and environmental factors in clay dune genesis. Journal of Sedimentary Research, 33(3), pp.766-778.

Rawlings, K., Freudenberger, D. and Carr, D., 2010. *A guide to managing box gum grassy woodlands*. Commonwealth of Australia.

Reinfelds, I., Swanson, E., Cohen, T., Larsen, J. and Nolan, A., 2014. Hydrospatial assessment of streamflow yields and effects of climate change: Snowy Mountains, Australia. Journal of Hydrology, 512, pp.206-220.

Rizal, Y., Westaway, K.E., Zaim, Y., van den Bergh, G.D., Bettis, E.A., Morwood, M.J., Huffman, O.F., Grün, R., Joannes-Boyau, R., Bailey, R.M. and Westaway, M.C., 2020. Last appearance of Homo erectus at Ngandong, Java, 117,000–108,000 years ago. Nature, 577(7790), pp.381-385.

Rosenzweig, R. and Porat, N., 2015. Evaluation of soil-moisture content for OSL dating using an infiltration model. Ancient TL, 33(2), pp.10-14.

Saini, S., Jackson, N.L. and Nordstrom, K.F., 2012. Characteristics of sediment in transport in the swash zone of a steep estuarine foreshore. Sedimentology, 59(3), pp.1001-1013.

Sankey, J.B., Kasprak, A., Caster, J., East, A.E. and Fairley, H.C., 2018. The response of source-bordering aeolian dunefields to sediment-supply changes 1: effects of wind variability and river-valley morphodynamics. Aeolian research, 32, pp.228-245.

Scanlon, B.R., Keese, K.E., Flint, A.L., Flint, L.E., Gaye, C.B., Edmunds, W.M. and Simmers, I., 2006. Global synthesis of groundwater recharge in semiarid and arid regions. Hydrological Processes: An International Journal, 20(15), pp.3335-3370.

Schewe, J., Heinke, J., Gerten, D., Haddeland, I., Arnell, N.W., Clark, D.B., Dankers, R., Eisner, S., Fekete, B.M., Colón-González, F.J. and Gosling, S.N., 2014. Multimodel assessment of water scarcity under climate change. Proceedings of the National Academy of Sciences, 111(9), pp.3245-3250.

Schnurrenberger, D., Russell, J. and Kelts, K., 2003. Classification of lacustrine sediments based on sedimentary components. Journal of Paleolimnology, 29(2), pp.141-154.

Sherman, D.J., Nordstrom, K.F., Jackson, N.L. and Allen, J.R., 1994. Sediment mixing-depths on a low-energy reflective beach. Journal of Coastal Research, pp.297-305.

Slavich, P.G., Walker, G.R., Jolly, I.D., Hatton, T.J. and Dawes, W.R., 1999. Dynamics of Eucalyptus largiflorens growth and water use in response to modified watertable and flooding regimes on a saline floodplain. Agricultural Water Management, 39(2-3), pp.245-264.

Stanica, A. and Ungureanu, V.G., 2010. Understanding coastal morphology and sedimentology. Terre et Environnement, 88, pp.105-111.

Thomsen, K.J., Murray, A. and Jain, M., 2012. The dose dependency of the over-dispersion of quartz OSL single grain dose distributions. Radiation Measurements, 47(9), pp.732-739.

Udden, J.A.,1914. Mechanical composition of clastic sediments. Bulletin of the Geological Society of America, 25, 655–744.

Van Der Wal, D., 1998. The impact of the grain-size distribution of nourishment sand on aeolian sand transport. Journal of Coastal Research, pp.620-631.

Wasson, R.J. and Hyde, R., 1983. Factors determining desert dune type. Nature, 304(5924), pp.337-339.

Wentworth, C.K., 1922. A scale of grade and class terms for clastic sediments. The journal of geology, 30(5), pp.377-392.

Waternsw.com.au. 2021. Real-time data. [online] Available at: <https://www.waternsw.com.au/waterinsights/real-time-data> [Accessed 2 August 2021].

Wintle, A.G. and Murray, A.S., 2006. A review of quartz optically stimulated luminescence characteristics and their relevance in single-aliquot regeneration dating protocols. Radiation measurements, 41(4), pp.369-3

W. L. Gore & Associates, 2006. Geochemical survey of the Griffith area, New South Wales, Australia. Client report prepared for NSW Department of Primary Industries (unpublished).

8. Appendix

8.1 Water balance calculation results table

Catchment size (km 2)			69									
Lake Sunrise size (outer, km2)			7.2									
Lake Sunrise size (inner, km2)			1.15									
Outer Lake	P	E	Aridity Index (P/E)	Runoff factor	Catchment surface runoff (m3)	Runoff converted to mm on lake surface	Sunrise direct precipitation (mm/year)	Evap lake sunrise (mm/year)	annual balance (mm) (runoff+preci p-evap)	Total water into lake sunrise basin	Lake bed area (m2) / Total surface input	Conversion to mm
	500	2500	0.2	0.05	1545000	214.583333	500	2500	-1785.416667	1542040	0.2142	214.1722222
Outer Lunette Lake (Current, P 500, E 2000)	500	2000	0.25	0.05	1545000	214.583333	500	2000	-1285.416667	1542300	0.2142	214.2083333
	500	1500	0.33	0.05	1545000	214.583333	500	1500	-785.4166667	1543616	0.2144	214.3911111
	500	1000	0.5	0.05	1545000	214.583333	500	1000	-285.4166667	1543300	0.2143	214.3472222
	500	750	0.67	0.05	1545000	214.583333	500	750	-35.41666667	1544366	0.2145	214.4952778
	500	500	1	0.05	1545000	214.583333	500	500	214.5833333	1544616	0.2145	214.53
Dry	250	2000	0.12	0.05	772500	107.291666	250	2000	-1642.708333	769790	0.1069	106.9152778
	250	1500	0.16	0.05	772500	107.291666	250	1500	-1142.708333	770050	0.107	106.9513889
	250	1000	0.25	0.05	772500	107.291666	250	1000	-642.7083333	771366	0.1071	107.1341667
	250	750	0.33	0.05	772500	107.291666	250	750	-392.7083333	770800	0.1071	107.0555556

	250	500	0.5	0.05	772500	107.291666	250	500	-142.7083333	771866	0.1072	107.2036111
	250	250	1	0.05	772500	107.291666	250	250	107.2916667			
Wet	750	2500	0.3	0.05	2317500	321.875	750	2500	-1428.125	2314790	0.3215	321.4986111
	750	2000	0.37	0.05	2317500	321.875	750	2000	-928.125	2315050	0.3215	321.5347222
	750	1500	0.5	0.05	2317500	321.875	750	1500	-428.125	2316366	0.3217	321.7175
	750	1000	0.75	0.05	2317500	321.875	750	1000	71.875	2316050	0.3217	321.6736111
	750	750	1	0.05	2317500	321.875	750	750	321.875	2317116	0.3218	321.8216667
	750	500	1.5	0.05	2317500	321.875	750	500	571.875	2317366	0.3219	321.8563889
Inner Lake Inner Lunette Lake Current (P 500 mm, E 2000 mm)	500	2500	0.2	0.05	1545000	1343.47826	500	2500	-656.5217391	1542040	1.3409	1340.904348
	500	2000	0.25	0.05	1545000	1343.47826	500	2000	-156.5217391	1542300	1.3411	1341.130435
	500	1500	0.33	0.05	1545000	1343.47826	500	1500	343.4782609	1543616	1.3423	1342.274783
	500	1000	0.5	0.05	1545000	1343.47826	500	1000	843.4782609	1543300	1.342	1342
	500	750	0.67	0.05	1545000	1343.47826	500	750	1093.478261	1544366	1.3429	1342.926957
	500	500	1	0.05	1545000	1343.47826	500	500	1343.478261	1544616	1.3431	1343.144348
Dry	250	2500	0.1	0.05	772500	671.739130	250	2500	-1578.26087	769290	0.6689	668.9478261
	250	2000	0.125	0.05	772500	671.739130	250	2000	-1078.26087	769550	0.6692	669.173913
	250	1500	0.16	0.05	772500	671.739130	250	1500	-578.2608696	770866	0.6703	670.3182609
	250	1000	0.25	0.05	772500	671.739130	250	1000	-78.26086957	770550	0.67	670.0434783
	250	750	0.33	0.05	772500	671.739130	250	750	171.7391304	771616	0.671	670.9704348
	250	500	0.5	0.05	772500	671.739130	250	500	421.7391304			

Wet	750	2500	0.3	0.05	2317500	2015.21739	750	2500	265.2173913	2314790	2.0129	2012.86087
	750	2000	0.375	0.05	2317500	2015.21739	750	2000	765.2173913	2315050	2.0131	2013.086957
	750	1500	0.5	0.05	2317500	2015.21739	750	1500	1265.217391	2316366	2.0142	2014.231304
	750	1000	0.75	0.05	2317500	2015.21739	750	1000	1765.217391	2316050	2.014	2013.956522
	750	750	1	0.05	2317500	2015.21739	750	750	2015.217391	2317116	2.0149	2014.883478
	750	500	1.5	0.05	2317500	2015.21739	750	500	2265.217391	2317366	2.0151	2015.10087

8.2. Radial plots

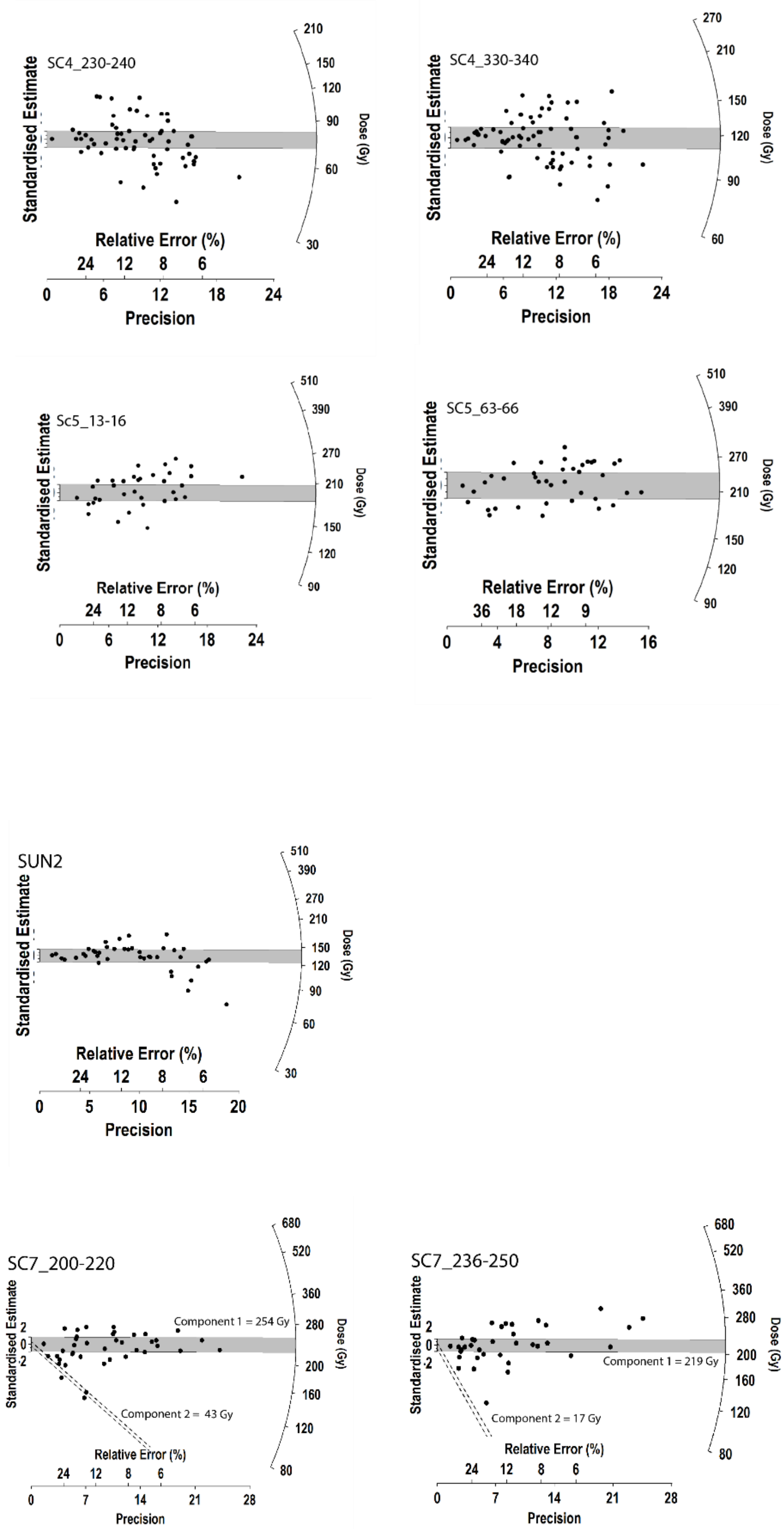

Appendix 8.2.1 – Radial plots of equivalent dose (De) determined from OSL age analysis of Lake Sunrise sediment samples. The black dots represent the measured equivalent dose of individual grains. The Y-axis shows the relative error and precision of individual grains, whilst the X-axis shows the measured equivalent dose.

Appendix 8.3 – FMM Output

SC7_220-240

number of components: 2 llik: -36.2574 BIC: 83.581 30%

[,1] [,2]

dose 42.4653 239.1650

re 0.1562 0.0594

[,1] [,2]

prop 0.1813 0.8187

se 0.0641 0.0641

SC7_236-250

number of components: 2 llik: -40.6712 BIC: 92.093

[,1] [,2]

dose 16.8805 219.0218

re 0.5247 0.1178

[,1] [,2]

prop 0.0783 0.9217

se 0.0525 0.0525

SC7_270-280

number of components: 2 llik: -45.9637 BIC: 103.211 60%

	[,1]	[,2]
dose	42.9278	254.2926
re	0.6042	0.1076

	[,1]	[,2]
prop	0.0577	0.9423
se	0.0528	0.0528

Appendix 8.4Table 3.1.1 Extended	Sample ID									
Rejection criteria	SC7_270-280	SC5_50-59	SC4_240-250	SC4_330-340	SC4_230-240	SC7_200-220	SC7_236-250	SC5_13-16	SC5_63-66	SUN2
Total Grains	900	600	500	700	500	600	700	800	900	1200
Initial rejection phase*										
Poor signal <3 >sd bg[a] (%)	54.8 %	10.8 %	23.2 %	28.4 %	21.7 %	50.1 %	48.7 %	15.8 %	14.4 %	10.2 %
Recycling ratios > or < 0.8-1.2[b]	56.2 %	38.2 %	72.4 %	54.3 %	60.4 %	51.1 %	55.5 %	40.8 %	43.6 %	24.9 %
Recuperation >5 % [c]	38.5 %	4 %	12.8 %	9.8 %	15.4 %	43.2 %	44.4 %	8.1 %	6.8 %	14.3 %
Grains progressing to final dose response curve analysis	156	260	132	148	107	99	104	205	213	389
Super saturated [d]	72.3 %	63.1 %	25 %	28.4 %	26.3 %	70.4 %	68.3 %	60.4 %	58.6 %	22.2 %
Accepted grains	43	96	99	81	62	40	42	38	39	42
Total acceptance rate (%)	**4.8 %**	**11.5 %**	**19.8 %**	**11.5 %**	**12.4 %**	**6.6 %**	**6.0 %**	**4.75 %**	**4.3 %**	**3.5 %**

* Grains may be rejected on multiple criteria, reflective in the percentage of each rejection category.

[a] Observed natural signal exceeding background standard error (3SE).

[b] Recycling ratio exceeded acceptance range (0.8-1.2).

[c] Zero dose signal greater than natural signal.

[d] Natural signal projected outside of regenerative dose points.